An Investigation on Linear and Nonlinear Optical Properties of Pristine and Co doped MgO

Project report submitted to the

University of Kerala

In the partial fulfillment of the requirements for the award of the degree of

MASTER OF SCIENCE IN PHYSICS

2020-2022

CONTENTS

List of Figures

List of Tables

ABSTRACT

Magnesium oxide (MgO) nanoparticles are of special interest in research activity because of their astonishing properties in electronic devices due to their ferromagnetic nature, transparency to visible light and applications in catalysts, solar cells and solid oxide fuel cells. Thus doping of Co may be helpful in interpreting the effect of Co dopant in doped MgO. In this work, synthesis of nanostructures of MgO and Co doped MgO are done using modified auto combustion method using magnesium nitrate hexahydrate, cobalt nitrate hexahydrate and citric acid. Structural, morphological, and optical aspects together with third order optical nonlinearity have been investigated. The crystallite size of $Mg_{(1-x)}Co_xO$ $(x = 0, 0.01, 0.03, 0.05)$ are calculated as 10.62 nm, 12.48 nm, 13.19 nm, 13.52 nm respectively. Rietveld refinement confirms the structural parameters of the prepared nanoparticles. FE-SEM images confirm nanostructures with slightly agglomerated nature having flower petal like morphology. Chemical composition of the nanostructures is evaluated by using energy dispersive spectrum, confirms the presence of elements like magnesium, oxygen for pristine MgO and magnesium, cobalt, oxygen for doped samples. Linear optical behaviour of $Mg_{(1-x)}Co_xO$ $(x = 0, 0.01, 0.03, 0.05)$ can be identified from the UV-Visible absorbance spectrum. Using the Tauc plot calculations, bandgaps are evaluated and are found to be decreasing with doping concentration. The third order nonlinear properties of the prepared nanoparticles have been measured using the Z-scan method under diode pumped continuous wave laser with 532 nm wavelength. In open aperture Z-scan technique, combined effect of saturable absorption and reverse saturable absorption is observed on doping. On the other hand, a self-defocussing nature with negative refractive index is observed under closed aperture Z-scan method. Pristine MgO and Co-doped MgO are found to be superior candidates for the fabrication of optical limiting devices for protecting human eyes and other sensitive optical detectors from hazardous laser radiation.

Chapter-1

Introduction to Nonlinear Optics and Nanomaterials

1.1 Introduction to Non-linear Optics

Nonlinear optics is a branch of science, which deals with the interaction of intense light with matter. It is relatively a new field in physics with lots of scientific and technological applications. Here the interaction of electromagnetic fields with various materials generates new electromagnetic fields with different phase, amplitude, and frequency. Nonlinear optics is widely used in photonics and optoelectronic technology and is given increasing attention due to its wide applications in the area of laser technology, optical communication and data storage technology. With the rapid development of nanotechnology in the past few decades, a large number of nanomaterials have been shown to possess remarkable nonlinear optical properties which enhance the design and fabrication of nano and nano-scale photonic and photo electronic device.

After the invention of laser, it was recognized that laser beams are highly capable of causing damage to delicate optical instruments and human eye. Hence the protection of these instruments from laser induced damage became a scientific as well as a public issue. Therefore, the drastic growth of ultrafast and high intense laser in research and technology demands the ability to control the intensity of light in a predetermined and predictable manner. Thus optical limiters have received significant attention. An optical limiter is a device that strongly attenuates an optical beam to a threshold level at high intensity and exhibit linear transmittance at low intensity. MgO nanoparticles show good optical limiting property and are widely applicable.

Metal nanoparticles are nanoclusters of nanometer-dimension. These nano-sized metals have size in the range of 1-50 nm and are synthesized by different methods in liquids or in solids. Nano-crystal shows some peculiar properties such as surface plasmon absorption, IR photoluminescence, coulomb staircase, super magnetism, high chemical activities, ultrafast response, etc. For that reason, they are widely applied in drug delivery, as catalyst in chemical reaction, for optical limiting etc. Among the various metal oxides, Magnesium oxide (MgO) is considered to be a versatile material because of its wide band gap, excellent thermal stability, low dielectric constant and low refractive index, which finds extensive application in ceramics waste remediation, catalysis and in antibacterial materials.

Many techniques have been developed for the synthesis of nanoparticles, which are hydrothermal method, modified auto combustion method, sol-gel method etc. The present study focuses on the preparation of MgO by modified auto combustion method since it leads to the synthesis of crystalline particles with large surface area.

1.2. Nanomaterials

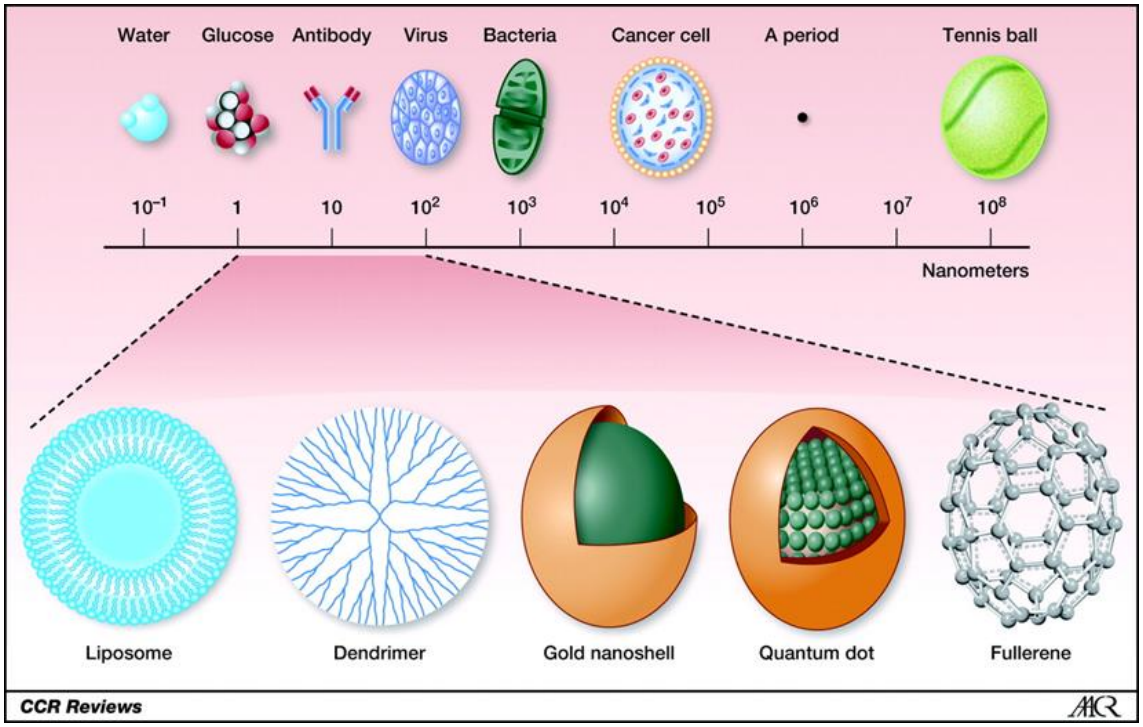

Fig 1.1 size variation of different nanoparticles

The nanoscale materials are defined as a set of substances where at least one dimension is less than approximately 100 nanometers. The nanomaterials are of interest because at this scale they possess unique optical, magnetic, electrical, and other properties emerge. These emergent properties have the potential for great impacts in electronics, medicine, and other fields.

Some nanomaterials occur naturally but for particular interest those are Engineered Nanomaterials (EN), which are designed for and being used in many commercial products and processes. They can be found in things as sunscreens, cosmetics, sporting goods, stain-resistant clothing, tires, electronics, as well as many other everyday items and are used in medicine for purposes of diagnosis, imaging, and drug delivery. Engineered nanomaterials are resources designed at the molecular (nanometre) level to take advantage of their small size

and novel properties which are generally not seen in their conventional, bulk counterparts. The two main reasons why materials at the nano scale can have different properties are increased relative surface area and new quantum effects. The nanomaterials have a much greater surface area to volume ratio than their conventional forms, which can lead to greater chemical reactivity and affect their strength. Also at the nano scale, quantum effects can become much more important in determining the materials properties and characteristics, leading to novel optical, electrical, and magnetic behaviors.

The nanomaterials are already in commercial use, with some having been available for several years or decades. The range of commercial products available today is very broad, including stain-resistant and wrinkle-free textiles, cosmetics, sunscreens, electronics, paints, and varnishes. The nanocoatings and nanocomposites are used in diverse consumer products, such as windows, sports equipment, bicycles, and automobiles. There are novel UV-blocking coatings on glass bottles which protect beverages from damage by sunlight, and longer-lasting tennis balls using butyl rubber/ nano-clay composites. Nanoscale titanium dioxide is used in cosmetics, sunblock creams, and self-cleaning windows and nanoscale silica is being used as filler in a range of products, including cosmetics and dental fillings.

1.3. Classification of Nanomaterials

The nanomaterials have extremely small size which having at least one dimension 100nm or less. The nanomaterials can be nanoscale in one dimension (eg. surface films), two dimensions (eg. strands or fibers), or three dimensions (eg.particles). They can exist in single, fused, aggregated, or agglomerated forms with spherical, tubular, and irregular shapes. Common types of nanomaterials include nanotubes, dendrimers, quantum dots, and fullerenes. Nanomaterials have applications in the field of nanotechnology and displays different physical chemical characteristics from normal chemicals (i.e , sliver nanoparticles, carbon nanotubes, fullerenes ,photocatalyst , carbon nanoparticles , silica) According to Siegel nanostructured materials are classified as zero dimensional, one dimensional, two dimensional, three dimensional nanostructures.The nanomaterials are materials which are characterized by an ultra-fine grain size (< 50 nm) or by a dimensionality limited to 50 nm.

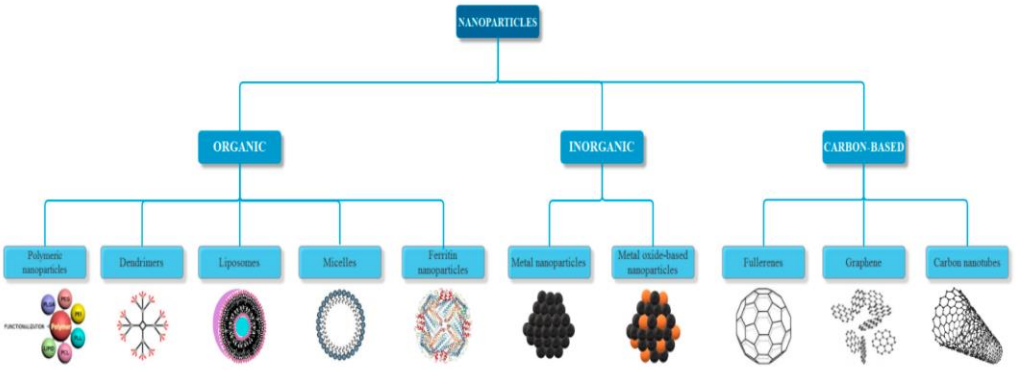

Fig. 1.2. Classification of nanoparticles

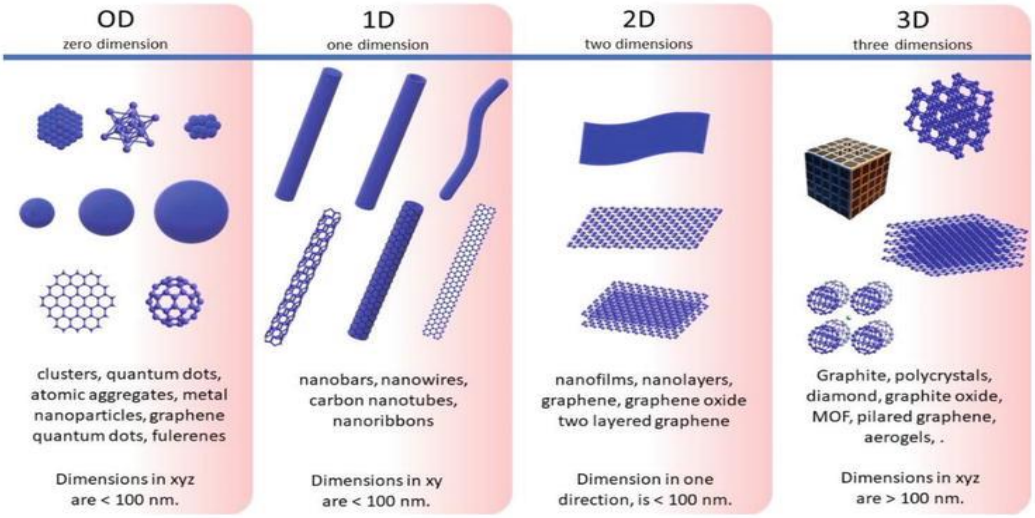

Fig. 1.3 Classification based on size

The nanomaterials can be created with various modulation dimensionalities as defined by Richard W. Siegel: zero (atomic clusters, filaments and cluster assemblies), one (multilayers), two (ultrafine grained over layers or buried layers), and three (nanophase materials consisting of equaled nanometer sized grains) as shown in the Fig. 1.2.

1.4 Optical Nonlinearity in Metal Nanostructures

Nanoparticles have interesting functional properties and also they have high surface energy due to large number of surface atoms. A wide range of nanoparticles have interesting optical properties. Optical properties of metal nanoparticles are primarily determined by the electrons

occupying the "d"and conduction band. Delocalization of electrons in the conduction band of a metal nanoparticle is only possible as long as the dimension of the particle is a multiple of electron's de Broglie wavelength. However, if a particle is smaller than the de Broglie wavelength, the electrons are localized between the atomic nuclei, so that they behave as typical molecules. Metal nanoparticle shows strong nonlinear response since they possess many highly polarizable electrons. Nonlinear optical susceptibility (χ) measured on nanostructures are considerably larger than in bulk metals. When the metallic nanoparticle is subject to light excitation, the electric field of the light induces waves of collective electron oscillations confined to the surface of the nanoparticle, a phenomenon known as a localized surface plasmon resonance (LSPR) (Link 2000, Kelly 2003, El-Sayed 2004 and Liz-Marzan 2006). This wave motion is composed of different orders, from the lowest dipolar to higher order multipole (Kelly 2003), depending on the size of the nanoparticles relative to the wavelength of the light. However, in the case of particles of size much smaller than the wavelength of the light, (i.e., radius $r << \lambda$), the nanoparticle feels a field that is spatially constant but with a time-dependent phase, known as the quasistatic limit. In this limit, the displacement of the charges in a sphere is homogeneous, yielding a dipolar charge distribution on the surface, while for larger spherical particles, high multipolar distributions are excited.

1.4.1 Basic Principles of linear and nonlinear optics

In linear optics, the optical parameters like refractive index, reflection, absorption, and transmission are assumed to be independent of the intensity of the light propagating through the media. Even though the electric field strength generated by the non-laser light sources is of the order 10^3 V/cm, it is very much smaller than the inter-atomic field of the medium (i.e 10^7 V/cm). Hence there is no effect on the atomic field of the medium and thereby the optical properties of the medium remain constant irrespective of the intensity of light. This is linear optics

By the invention of laser, the study of optics at high intensities became possible and that led to new phenomena not seen with ordinary beam of light such as generation of new colours from monochromatic light in a transparent crystal with altered phase, frequency and amplitude or the self-focusing of an optical beam in a homogeneous liquid. Optical properties of the materials cannot be considered constant at intensities but a function of light intensity

and is called nonlinear optics. When placed in an electric field, any dielectric medium becomes polarized if it does not have a transition at the frequency of the applied field. Then, with a dipole, each constituent molecule operates as a dipole with a dipole moment p_i,

The polarization *P* is given by the equation:

$P = \sum p_i$ …….(1.1)

Where, $\sum pi$ is the summation over the dipoles in the unit volume.

Nonlinear optical phenomena can be interpreted as a dielectric phenomenon. When electric fields like an applied dc field or a propagating electromagnetic wave passes through the medium, electron displacement is caused. The external applied electromagnetic field perturbs electrons bound to adjacent nuclei in the medium, causing them to oscillate at the applied frequency. At appropriate field strengths, the amplitude of such an induced polarization (P) will be proportional to the applied field and stated as **equation 1.2.**

$P=\varepsilon_0 \chi^{(1)}E$……(1.2)

where E is the magnitude of the applied electric field, $\chi^{(1)}$ is the polarizability of the material and ε_0 is the permittivity of the free space.

At sufficiently powerful applied fields, the nonlinear optical effect occurs. The polarization response of the medium is no longer linear when the applied field strength increases (e.g., lasers), as demonstrated by **equation 1.2. Equation 1.3** gives the microscopic induced polarization (P) as a function of the applied field.

$P= \Sigma \alpha_{ij}E + \Sigma \beta_{ijk}E^2 + \Sigma\gamma_{ijkl}E^3 +$ ..... (1.3)

where,

α_{ij} = Polarizability

β_{ijk} = First hyperpolarizability (*second order effects*)

γ_{ijkl}= Second hyperpolarizability (*third order effects*)

Macroscopic polarization induced in bulk media can be expanded in a power series in the external field as shown in equation **1.4** as given below.

$P = \varepsilon_0 \{\chi^{(1)}E + \chi^{(2)} E^2 + \chi^{(3)} E^3 + ...\}$ .....(1.4)

where $\chi^{(1)}$ is the linear term responsible for linear optical properties of materials like refractive index, dispersion, birefringence and absorption, $\chi^{(2)}$ is the quadratic term which describes second harmonic generation (SHG), $\chi^{(3)}$is the cubic term responsible for third harmonic generation (THG), stimulated Raman scattering, phase conjugation and optical bistability etc. and *i, j, k, l* corresponds to the molecular coordinates.

At the molecular level,**equation1.3** is expressed as **equation1.4** [6].

Here, $\chi^{(1)}$, $\chi^{(2)}$ and $\chi^{(3)}$ are the first, second and third order nonlinear optical susceptibilities and have similar meanings as their microscopic counterparts α,β *and γ.*

The molecules in a crystal that exhibit NLO response must have molecules with asymmetric charge distribution. If the molecule is centrosymmetric, first order hyperpolarizability (β) is zero, implying that second harmonic generation (SHG) is not possible. Only non-centrosymmetric media demonstrate SHG. This is explained as follows. If a field +E is applied to the crystal, equation 1.3 predicts the first nonlinear term as $+\beta E^2$. The polarization is still expected when a field –E is applied and the polarization is still predicted to be $+\beta E^2$. But the polarization of a centrosymmetric crystal (or molecule) with -E applied field should be $-\beta E^2$. This contradiction can be resolved only if the quantity $\beta = 0$. This indicates that the centrosymmetric crystal or molecule has zero β value. When it comes to the third order NLO susceptibility, +E field produces polarization $+\gamma E^3$ and –E field produces $-\gamma E^3$. So the second order hyperpolarizability (γ) is the first non-zero nonlinear term in centrosymmetric media.

If the incident light is represented by $E=E_0 \cos\omega t$, polarization P is given by,

$P = \varepsilon_0 \{\chi^{(1)} E_0 \cos\omega t + \chi^{(2)} E_0^2 \cos^2\omega t + \chi^{(3)} E_0^3 \cos^3\omega t + ...\}$ .....(1.5)

Using the relations in (1.5),

$P = 1/2\ \varepsilon_0\chi^{(2)}E_0^2 + \varepsilon_0 \{\chi^{(1)} + 3/4\chi^{(3)} E_0^2\} E_0 \cos\omega t + 1/2\ \varepsilon_0\chi^{(2)} E_0^2\cos^2\omega t + 1/4\ \varepsilon_0 \chi^{(3)} E_0^3\cos^3\omega t + ...\}$ …… (1.6)

The **equation.1.6** clearly shows the presence of new frequency components due to nonlinear polarization. In this equation, the first term is a constant term which gives rise to a dc field through the medium. The second term is the external polarization, called as first or

fundamental harmonic of polarization. The third term oscillates at a frequency of 2ω and is called second harmonic of polarization. The fourth term oscillates at a frequency of 3ω and is called third harmonic of polarization and so on. The contributions from the second and third order terms to the nonlinear polarization are predicted from different symmetry properties of the medium.A contribution from $\chi^{(2)}$can occur only from non-centrosymmetric media, whereas $\chi^{(3)}$contributions can occur from any medium regardless of symmetry.

1.4.2 Second Harmonic Generation (SHG)

In SHG, the incident radiated frequency $\omega_1$is convened to twice the frequency of the incident radiation ($\omega_2 = 2\omega_1$). The first SHG property was observed in 1961 by Franken and his coworkers (Franken et al., 1961). They focused a red ruby laser light (694.2 nm) on a quartz crystal and observed that light of 347.1 nm was generated by the quartz crystal. Though the discovery of SHG marked the birth of nonlinear optics, it was not the first observation of NLO effect. Optical pumping phenomenon was discovered prior to the invention of laser (Maiman, 1960).

In second harmonic generation, wave with a frequency ω generates a signal at the frequency 2ω as it propagates through a medium having quadratic nonlinearity. A polarization oscillating at frequency 2ωradiates an electromagnetic wave of the same frequency, which propagates with the same velocity as that of the incident wave. The wave thus produced has the same characteristics of directionality and monochromaticity as the incident wave and is emitted in the same direction. This phenomenon is known as the second harmonic generation (SHG).

Using a strong fundamental beam (= 1064 nm) of a pulsed Nd: YAG (Neodymium-doped Yttrium Aluminum Garnet; Nd:$Y_3Al_5O_{12}$) laser, the second harmonic production in a crystalline powder can be clearly detected. For the incident intense IR (infrared) beam on the powder, the SHG occurs as a scattered green light (λ= 532 nm). Since the genesis of optical nonlinearities is electronic and the in electric dipole approximation only the valance electrons contribute to the nonlinear susceptibility of the second order, the magnitude of the nonlinear coefficient depends upon the direction of the electronic wave functions and the asymmetry of the electron clouds. Therefore, non-centrosymmetric crystals exhibit good SHG.

1.4.3 Third order NLO Processes

The third order nonlinearity is usually studied in centrosymmetric media where$\varepsilon\,\chi^{(2)}$ is zero. Some of the important third order nonlinear effects are

- Third Harmonic Generation (THG)
- Raman Scattering
- Non-degenerating four wave mixing
- DC Kerr effect
- Brillion scattering
- Two photon absorption

These processes are highly important since they can be used for photonic applications such as all-optical switching(AOS) and optical power limiting (OPL), both of which are particularly important as laser systems are ubiquitous in information and communication technologies. Z-scan procedure is a simple and versatile tool to determine the third order nonlinear properties such as nonlinear refractive index (n_2) and nonlinear absorption (β) of solids and liquids. It was developed to measure the magnitude of n_2 and β simultaneously at the same time. Sign of nonlinear refractive index can also be obtained.

Processes originating from $\chi^{(3)}$ are described in this section. Regardless of spatial symmetry, $\chi^{(3)}$ is non-vanishing in any material and is responsible for a number of optical phenomena . Third order contribution to nonlinear polarization is given by

$$P^{(3)}(\omega_4)= \chi^{(3)}(\omega_4;\omega_1,\omega_2,\omega_3)E(\omega_1)E(\omega_2)E(\omega_3) \quad (1.7)$$

Based on the values of frequencies ω_1, ω_2, and ω_3, the interaction with an NLO material can give rise to third order NLO processes such as third harmonic generation, quadratic electro-optic effect (or Kerr effect), four wave mixing, two photon absorption, intensity dependent refractive index *etc*.

When $\omega_1 = \omega_2 = \omega_3 = \omega$ and $\omega_4 = 3\omega$, the polarization, $P^{(3)}(\omega_4 = 3\omega)$, is the source of third harmonic generation (THG) and is given by

$$P^{(3)}(3\omega)= \chi^{(3)}(3\omega;\omega,\omega,\omega)E^3(\omega) \quad (1.8)$$

When $\omega_1 = 0$ (dc or low frequency ac field) and $\omega_2 = \omega_3 = \omega$, the process is known as electric field induced second harmonic generation (EFISHG) and is represented by

$$P^{(3)}(2\omega) = \chi^{(3)}(2\omega;0,\omega,\omega)E(0)E^2(\omega) \quad (1.9)$$

One of the incident fields is a dc field and the second harmonic generation can be induced by this technique even in materials having inversion symmetry.

When, $\omega_1 = \omega_2 = \omega$, $\omega_3 = \omega$ and $\omega_4 = -\omega$, the process is referred to as degenerate four wave mixing and it can be represented by

$$P^{(3)}(\omega) = \chi^{(3)}(-\omega;\omega,\omega,\omega)E^3(\omega) \quad (1.10)$$

Four-wave mixing involves the interaction of four coherent optical beams in a nonlinear medium. Three of them are input waves and the fourth one is generated due to third order processes. If the frequencies of the incident fields are different from each other, then the process is known as non-degenerate four wave mixing. The four wave mixing process leads to important phenomena like optical phase conjugation.

Two photon absorption (TPA), a third order NLO process, corresponds to the simultaneous absorption of two photons of the same energy (degenerate TPA) or different energies (non-degenerate TPA), in the presence of intense radiation. The TPA process is characterized by $\chi^{(3)}(-\omega_1; -\omega 2, \omega_2, \omega_1)$. At very high intensities, the possibility of a material absorbing more than one photon before decaying to the ground state can be highly inflated. Two-photon absorption involves a transition from the ground state of a system to a higher lying state by the simultaneous absorption of two photons from an incident radiation field.

1.4.4 Optical Power Limiting Measurements

Optical limiters rely on materials exhibiting one or more optical limiting mechanisms, such as nonlinear absorption, nonlinear refraction, and induced scattering. Nonlinear absorption may result from multiphoton absorption (MPA), reverse saturable absorption (RSA), excited state absorption or free-carrier absorption (FCA) and free-carrier absorption associated with TPA.

Nonlinear refraction may be associated with molecular orientation, the optical and/or electronic Kerr effect, excitation of the free-carrier, photorefraction or optically induced heating of the material. Induced scattering is typically a consequence of plasma generation produced by optical heating. In this dissertation, only the nonlinear absorption mechanism that is related to optical limiting of nanostructured materials is covered.

The invention of lasers revolutionized science and technology, allowing for a wide range of uses in research, industry, medicine and military. The powerful and widespread sensors and optical components are better protected with wavelength range laser sources against high intensity components and human eyes. The main purpose of the protective device is to prevent dangerous intensity from reaching the sensor. The device should have excellent linear transmission at low intensity light so that some parts of the ambient light transmit through the material.

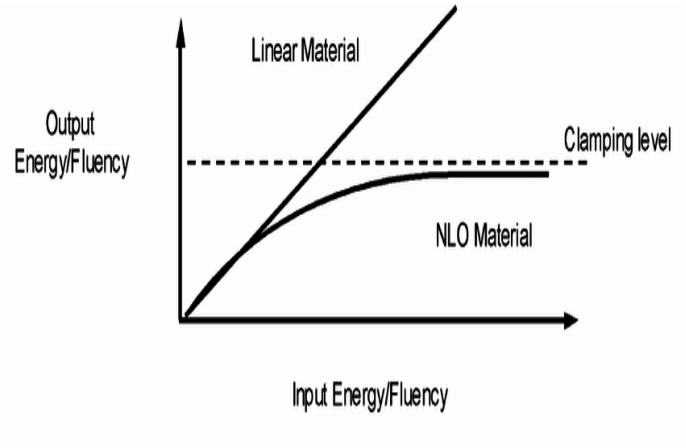

Fig 1.4: Schematic diagram represents the optical limiting behaviour of linear and nonlinear optical materials

The transmitted power decreases after a threshold value known as limiting threshold and it begins to deviate from the linear regime. The limiting threshold can be defined as the incident power at which the sample transmittance falls to 50% of the linear transmittance. When we increase the input power further, clamping of input power takes place because of the saturation of the transmitted power to a constant value. This phenomenon is known as optical clamping.

The general features of an optical limiting device are:

- Good mechanical, thermal and chemical stability
- Broad band response
- low input threshold
- High linear transmissions at low energies
- high attenuation
- quick recovery
- fast response
- High damage threshold

The output energy transmittance versus input intensity for an ideal optical limiter is shown in **Fig 1.4**. The physical mechanisms responsible for optical limiting properties can be divided in two different classes of optical nonlinearities viz. instantaneous and accumulative nonlinearities. In an instantaneous process, the polarization resulting from an applied optical field occurs immediately whereas accumulative nonlinearities arise when the induced nonlinear polarization either develops or decays on a time scale comparable to or longer than the excitation duration. In other words, the instantaneous nonlinearity depends on the instantaneous intensity within the medium whereas the accumulative nonlinearity is dependent on the energy density, fluence, deposited on the medium. Two-photon absorption (TPA) is an instantaneous process whereas excited state absorption (ESA) and nonlinear refraction are examples of accumulative processes associated with optical limiters. A material that shows optical limiting properties generally exhibits several different mechanisms that work together. The most important mechanisms in optical limiting is two photon absorption (TPA), reverse saturation absorption(RSA) and nonlinear refraction.

1.4.5 Two Photon Absorption (TPA) $\chi^{(3)}$ $(-\omega_1; -\omega_2, \omega_2, \omega_1)$

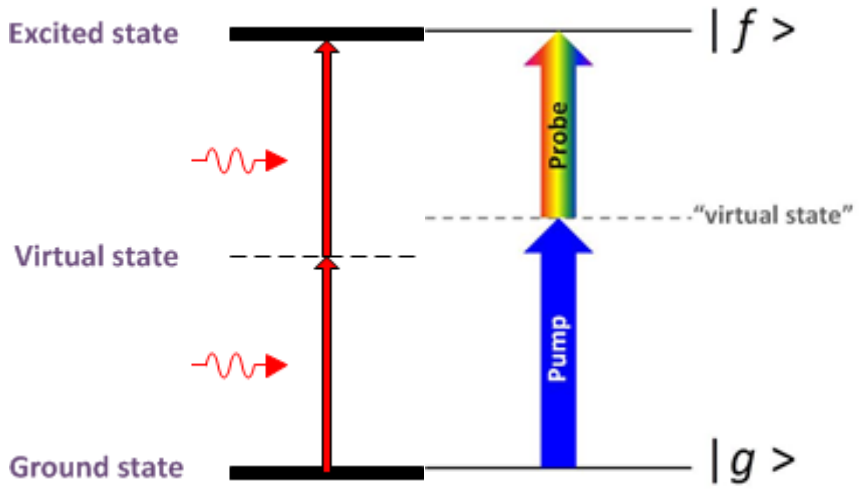

(a) (b)

Fig 1.5: schematic diagram of **(a)** self and (**b)** pump-probe two photon absorption process

When an incident radiation field passes through a medium, transition from the ground state to a higher lying state takes place by the simultaneous absorption of two photons. This process is known as two photon absorption. The strength of TPA depends on the square of the light intensity, thus it is a nonlinear optical process. Here, absorption of two photons takes place from the same optical field of frequency ω such that the transition takes place to an excited state resonance at 2ω.

Intermediate state (or virtual state) is not real (i.e., does not involve real stationary state of the system) in this case. Hence the system must absorb the two photons simultaneously. This makes the process sensitive to the instantaneous optical intensity. Although the transition does not involve a real intermediate state, often there are impurities present that will produce a small amount of linear absorption. It should be understood that this absorption does not contribute to the transition to the final state of the process but only serves as an additional loss mechanism. On the other hand, the two-step absorption involving a single photon pumped intermediate state is described as excited state absorption.

There are two possible ways of two photon absorption that is shown in the **Fig. 1.5**. In **Fig.1.5 (a)**, two photons from the same incident field oscillating at a frequency $\omega_1$areabsorbed to make

a transition. In **Fig. 1.5(b)**, two fields viz. pump and probe beam are incident on a medium and one photon from each field with frequency ω_1 and $\omega_2$are absorbed for the transitions respectively. In these two figures, the virtual state is not a real state (*i.e.*, it does not involve a real stationary state and the system absorbs two photons simultaneously). This process is sensitive to the instantaneous optical intensity.

1.4.6 Nonlinear Absorption

The optical properties of a material changes abruptly when it is exposed to intense monochromatic radiation. If the absorption occurs nonlinearly, the transmittance of the material changes as a function of intensity. If the incident intensity is greater than the saturation intensity, the population of the excited state increases significantly. In polyatomic molecules and semiconductors, a high density of states is present near the state that is involved in the excitation. The excited electrons can rapidly transit to one among these states before it reaches the ground state. Similarly there are a number of excited states that couples radiatively with these intermediate states. The excited state energy differences are in near-resonance region with the incident photon energy. Therefore, before the electrons transit to the ground state, they may experience absorption and get excited to a higher-lying state and this type of process is called excited state absorption (ESA). This type of process occurs when the input intensity is strong enough to deplete the ground state.

If the ground state absorption cross section is greater than the absorption cross section of the excited state i.e. , if $\sigma_e << \sigma_g$, then it results in enhanced transmission of the system and the process is called as saturable absorption (SA). The system will be less transmissive when $\sigma_e >> \sigma_g$ and this process is called reverse saturable absorption (RSA). In Two Photon Absorption (TPA), simultaneous absorption of two photons takes place through an intermediate virtual state in the medium.

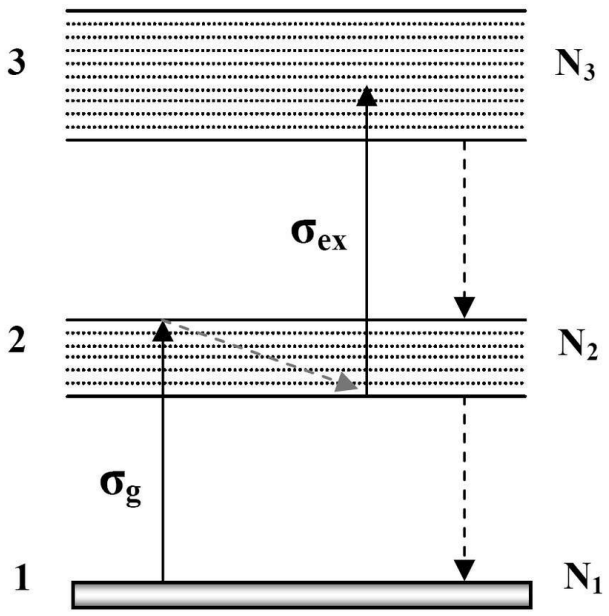

Fig 1.6 :energy level diagram of saturable and reverse saturable absorption

1.4.7 Excited state absorption

The excited state becomes populated when the incident intensity is sufficient to deplete the ground state. In systems as polyatomic molecules or semiconductors, there is a high density of states close to state involved in the excitation. These excited electrons rapidly make a transition to one of these states before it eventually transit backs to the ground state. However, there may be a number of higher-lying states that are coupled to these intermediate states and have energy differences that are close to the incident photon energy. As a result, it may experience absorption before the electron completely relaxes to the ground state, which promotes it to the higher-lying state. This process is called excited state absorption.

1.4.8 Saturable Absorption (SA)

Saturable absorption (SA) takes place when the absorption cross section of an excited state is smaller than that of the ground state. As photons from the incident light beam pump electrons into the upper energy levels, the ground state becomes depleted. The population in the upper state can undergo spontaneous and stimulated emission of photons. As a result, the

system cannot absorb the incident light as it does at lower intensities. Thus there is an intensity dependent reduction in the absorption coefficient of the two level systems. This process is called Saturable Absorption (SA). Saturable absorption (SA) occurs when the absorption cross-section of the excited state is smaller than that of the ground state. The materials with SA usually have a negative nonlinear absorption coefficient.

1.4.9 Reverse Saturable Absorption (RSA)

Reverse Saturable Absorption (RSA) occurs in a molecular system, when the excited state absorption cross section is larger than the ground state absorption cross section. Such a system will have an improved absorption capability and will be less transmissive when excited. Materials with a positive nonlinear absorption coefficient exhibit reverse saturable absorption and are characterized by high transmission at normal light intensities and decrease their transmission under high intensity or fluence. In inorganic nano materials, RSA occurs when ESA outperforms the ground state absorption. This will decrease the transmission with increase in the incident light intensity. Both saturable and reverse saturable absorption may occur in the same molecule. Some times RSA may even predominate SA.

1.5 Nonlinear Refraction

Nonlinear refraction is the phenomenon in which the refractive index of the medium varies at high intensity or fluence. When a high intensity light is allowed to fall on an NLO-material, a refractive index change is noticed. This change can be seen as either positive or negative and cause the material to either defocus or focus the light as shown in the **Fig.1.7**.For negative nonlinearities, the beam will not collapse but rather will diverge due to the negative lens effect. And for positive nonlinearities, beam will converge due to positive lens effect.

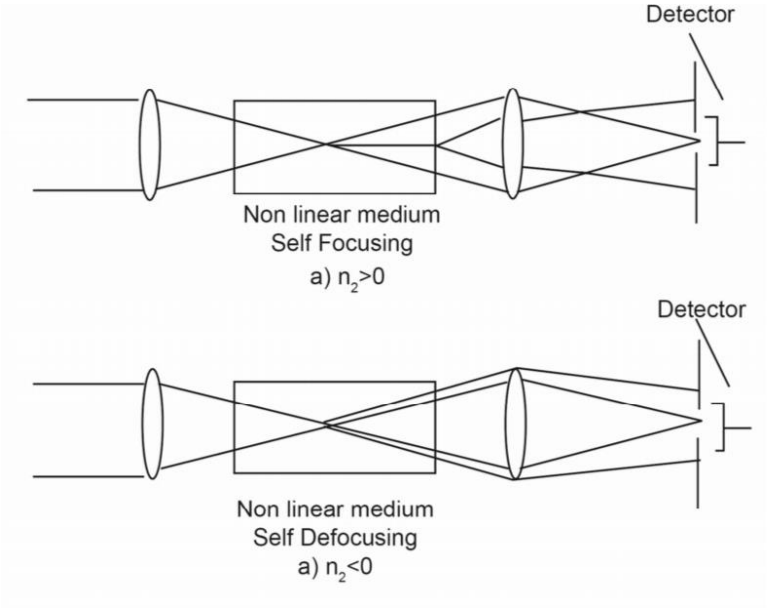

Fig 1.7: Optical limiter based on self-focusing (a) $n_2 > 0$ and (b) $n_2 < 0$

Self-focusing cause laser damage, so it is undesirable. The most common device application is optical limiting. Between the two lenses, there is a nonlinear medium. Low intensity light is collected by the second lens and imaged through an aperture to a detector. High-intensity light will produce self-focusing. For $n_2 > 0$; this will result in beam collapse and phase distortion such that the light is not focused by the second lens but defocused in the aperture plane. Thus the power transmitted by the aperture to the detector is limited, and the detector is thus protected from the high-intensity radiation. In the negative $n_2$case, the beam diverges more rapidly from the intermediate focus rather than collapsing. The result at the aperture plane is, however, the same: a defocused beam. The advantage of this type of limiter over the previous example is that it is self-protecting (*i.e.*, the light is defocused inside the medium leading to lower intensity there that is less likely to cause laser damage). This is important when the medium is solid and the damage would be permanent.

1.6 Synthesis of nanomaterials

The first step in the nano technology is the fabrication of nanomaterials and nano structures. Fabrication is very important in getting better knowledge of different nanoparticles and understanding its physical chemical and biological properties. The nanomaterials synthesis methods can be classified in to two approaches.

- Top down approach
- Bottom up approach

In the bottom up approach nano materials are synthesized by the self-assembly of atoms and molecules according to a natural physical principle or an externally applied driving force, to give rise to larger and more organized systems. In the top down approach the bulk material is splitted up in to nanoparticles .The three main categories of nanomaterial synthesis are vapour phase, liquid phase and solid phase. They are also classified in to physical chemical and biological methods ,solid state synthesis methods are widely used in industrial field. Liquid phase synthesis methods involve the precipitation of the nanoparticles from a solution Eg: Sol gel synthesis, Pyrolysis is an example of vapour phase synthesis methods

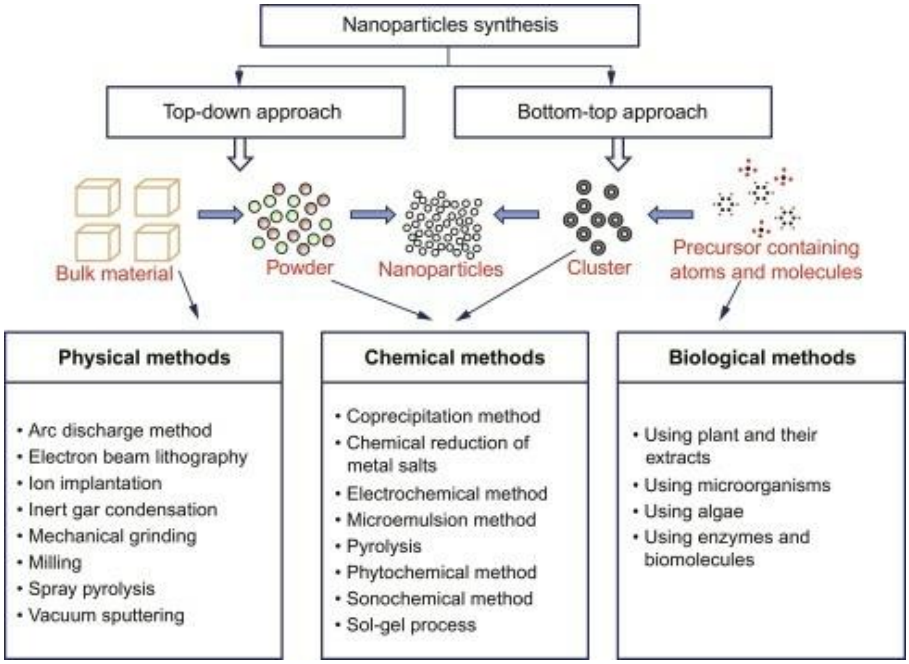

Fig:1.8 Synthesis of nanomaterials

1.7 Physical methods

1.7.1 High energy ball milling

Ball milling process has been so long to reduce size in various industries .High energy ball milling a process by which a powdered material is placed in the ball mill subjected to collisions with high energy from balls. This technique can be used to produce nano rods, nanowires and

nanotubes. This technique is also capable of inducing structural changes and reactions at room temperature. The behaviour of powder particles during milling can be distinguished in three ways

- Mechanical alloying
- Mechanical milling
- Mechanical chemical synthesis

Mechanical milling is when mixtures of powders are milled together. Mechanical milling defines process of milling when material transfer is not happened .In this powder with uniform composition is milled. Mechano-chemical reactions take place during milling. The advantage of processing nanomaterials by high energy ball milling includes versatility, effective coast, large quantity production.

1.7.2 Ion beam method

Ion beam method of synthesis is studied foe the embedded metallic nanocrystals. In this process a foreign element is introduced in the hoast matrix region. In this based first cluster is produced using laser. Next an ion beam ionizes the clusters, which are then accelerated towards a substrate, and clusters are deposited in thin film form, which are stable.

1.7.3 Laser ablation

It is a method used for fabricating various nanoparticles like quantum dots, carbon nano tubes, nanowires etc. The ablation means the removal of atom in the surface. In the nucleation and growth of laser vaporized species in a background gas is used to prepare nanoparticles.

1.8 Chemical Methods

1.8.1 Sol-gel Synthesis

The sol-gel synthesis is a wet chemical synthesis also known as chemical solution deposition. This method is used to prepare ceramic as well as glass material .At first a colloidal suspension of particle is prepared from a solution and it is called "sol". The gelation of sol form a network in a continuous liquid phase and is called "gel" .In the sol-gel preparation, the precursors (either organic or inorganic) undergo chemical reaction: hydrolysis and condensation or

polymerization, typically with acid and base as catalysts to form small solid particles or clusters in liquid. The starting materials used in the preparation of the sol are usually inorganic compounds such as metal oxides. In a typical sol-gel process, the precursor is subjected to a series of hydrolysis and polymerization reactions to form a colloidal suspension, or a “sol”. When the “sol” cast in to a mold, a wet “gel” will form. If the liquid in a wet “gel” is removed under a super critical condition, a highly porous and extremely low density material called “aerogel/ xerogel” is obtained. Sol-gel enables materials to be mixed on an atomic level and thus crystallization and densification to be accomplished at a much low temperature. The advantages of the sol-gel process in general are high purity, homogeneity and it is a low temperature process.

1.8.2 Hydrothermal process

Hydrothermal synthesis is one of the most commonly used methods for preparation of nanomaterials. It is basically a solution reaction-based approach. In hydrothermal synthesis, the formation of nanoparticles can happen in a wide temperature range from room temperature to very high temperature .To control the morphology of the materials prepared; either low-pressure to high-pressure condition can be used depending on the vapour pressure of the main composition in the reaction.

Hydrothermal method for nanoparticles synthesis requires using special equipment, known as hydrothermal autoclave reactor. It is a particular type of strengthened vessel which is designed to withstand high temperature and higher pressure levels from within. The autoclave consists of thick, steel-walled cylindrical vessel which is designed to withstand high temperature and higher pressure levels from within. Also, the material of the autoclave needs constant resistant to solvents. The process needs constant maintenance of temperature difference between the opposite ends of the crystallizing compartment. The end with higher temperature is where the solvent dissolved, while the other end, which is comparatively cooler, is where the nano particle growth takes place.

1.8.3 Combustion Process

Combustion is an extremely effortless process for the synthesis of nanocrystalline metal oxides and processing of advanced ceramics (structural and functional), catalysts, composites,

intermetallic and alloys. It is materialized to be a bottom-up approach and one such approach is also known as ‘self-propagating high temperature synthesis’ (SHS) and fire or furnace-less synthesis. In this process, the preferred products nucleate and grow from the combustion residue. Combustion can be treated as the ancient age technology of the mankind. As per the literature, Goldschmidt (1861-1923) was first to discover a method for igniting thermite without explosion, where thermite reaction is a method of extracting metals by reducing the oxides with carbon or aluminum powder and is a classical example of combustion reaction .

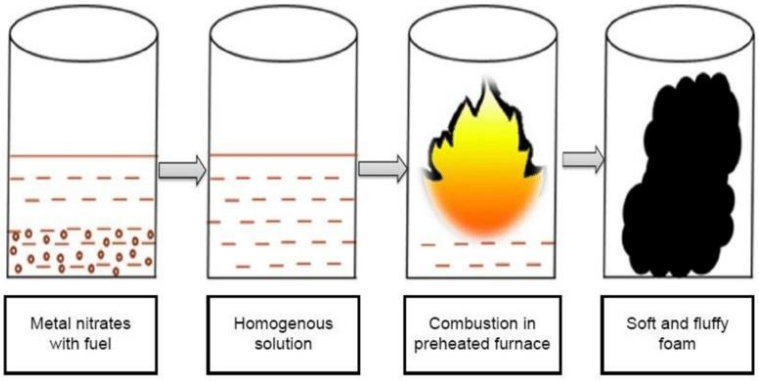

Fig: 1.9 Combustion process

During 1960s I. P. Borovinskaya, V. M. Skhiro and A. G. Merzhanov a group of researchers from Institute for Chemical Physics, U.S.S.R. Academy of Sciences, discovered “The phenomenon of the wave localization of solid-state auto retarding reactions”, which lead to the development of Second Harmonic Synthesis (SHS). A. G. Merzhanov, is the main pioneer and initiator of SHS a new science and he coined the name of SHS as structural

1.8.3.1 Classification of the combustion process

Based on the nature of reactants, reaction medium and the exothermicity , combustion synthesis is broadly classified into two courses namely solid state combustion and solution combustion synthesis process.

- The combustion process being simple is characterized by high-temperatures, fast heating rates and short reaction times.
- These features make combustion synthesis an attractive method for the production of technologically useful materials at low cost.

- The short exothermic reaction results in low operating and processing costs.
- It generally needs simple equipment and high-purity with any shape and size products are formed.
- The high thermal gradients and rapid cooling rates can produce a new non-equilibrium or stabilized metastable phases.
- Mixed metal oxides can be synthesized and consolidate.

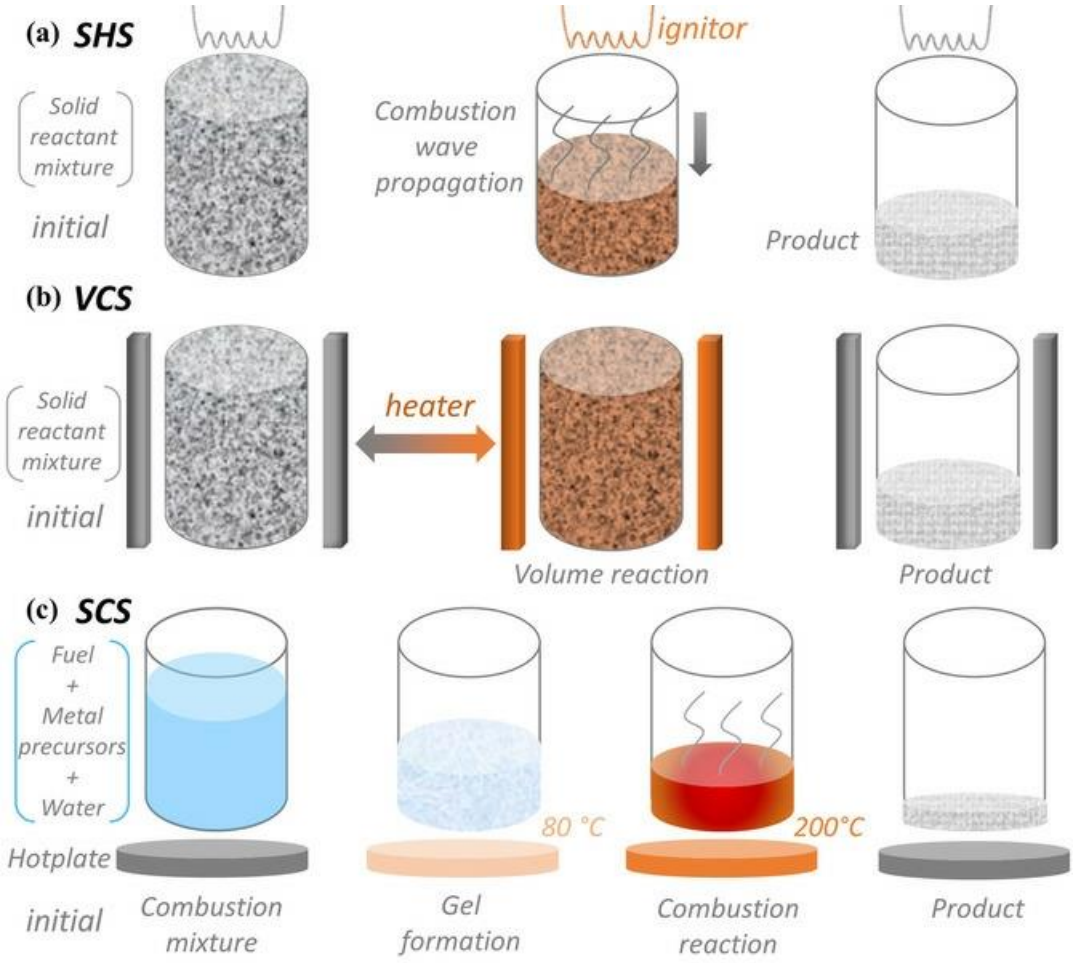

Fig 2.0: classification of combustion process based on reactants

1.8.3.2 Sol-Gel- auto-Combustion Method

This is one of the simple and cost effective method which involves both chemical and physical process. It is extensively used for the preparation of a various mixed metal oxide nanoferrites.

During combustion process flame temperature may vary from 600^0 C to 1350^0 C. In this method selection of proper complexing agent for phase formation is very important.

Stoichiometric ratio of desired metal ions and fuel as 1:3 ratios are mixed in distilled water and gives aqueous solution (sol).pH of the solution is maintained at 7 by adding the ammonia in the form of drops.

Homogeneous solution can be obtained by putting the aqueous solution on the magnetic stirred maintained at 50 ^{0}C. The resulting solution is evaporated gradually at 100^0C with constant stirring till the viscous xerogel (gel) produced .Temperature of gel is raised and at specific temperature, self-ignition of gel occurs with the development of fumes and fluppy powder. The burned gel is grinded to get a fine nanocrystalline powder. Finally this powder is sintered and the prepared samples are analyzed by using different characterization techniques.

Advantages of sol-gel auto combustion method

- Starting materials with fixed properly
- fine chemical uniformity'
- High purity of product
- Crystalline nature of synthesized materials
- Nanosized particles
- Maintains high stoichiometry of the product
- Simple method that do not require sophisticated equipments.
- Multiple steps are not required

1.8.4 Chemical Vapour Deposition

Chemical vapour deposition is a chemical process used to produce high purity nano structured materials .This technique is used in the semiconductor industry to produce thin films. In this chemical components in vapour phase react to form a solid thin film at substrate. The CVD deposition process is a two-step process one is a transport of gaseous materials to their reaction zone and other is the formation of film on the substrate. Based on the operating pressure in CVD it can be classified into

1. Atmospheric pressure CVD
2. Low pressure CVD

3. High pressure CVD

1.8.5 Biological methods

The micro-organisms, bio-templates and plant extract are also used to synthesize nanoparticles biologically. The bacteria and fungi can be used in the production of nanoparticles and is called biosynthesis. They allow production of nanoparticles in large scale with few impurities. The natural strains and plant extract secrete some photochemical set as both reducing agent and stabilizing agent. These approach low cost and environment friendly.

1.9 Literature review

Abed, S et al [1] prepared MgO doped thin films on a glass substrate by dip coating Technique. The grown films were then annealed at higher temperature of 500 °C for 6 hours. The optical and nonlinear optical properties of the MgO doped Co were characterized to be strongly dependent on the Co contents. Optical transmittance measurements indicated that all films have average 85% transparency in the visible region and the optical band gap of the films was found. Finally, the results of the third order nonlinear susceptibilities were calculated. Highly transparent MgO doped Co thin films have been obtained by dip coating technique. The effect of the Co concentration on the optical and nonlinear optical properties of MgO thin films was investigated. The transmission spectra show a high transmittance in the visible range. The maximum optical band gap value is found to be 3.97 eV. The Mg-O phase formation was identified from the FTIR results. The THG response has been measured; the highest third nonlinear susceptibility has been found for un-doped MgO.

Fahimeh Abrinaei et al [2], The results show that Mg/MgO structures synthesized in acetone and isopropanol have negative nonlinearity as well as good nonlinear absorption at 532 nm and these magnesium-based structures have the potential applications in the nonlinear optical devices.n this paper, two kinds of pulsed laser sources, an acousto-optically Q-Switched Nd:YAG laser, and a copper vapor laser (CVL) were used separately to vaporize the Mg metal target in isopropanol liquid medium. The compositions and structures of synthesized material were investigated by FTIR spectrum, X-ray diffraction (XRD), and Scanning Electron Microscopy (SEM). Formation of Mg and MgO nanocrystals by both kinds of lasers was recognized by XRD analysis and the obtained results from different lasers were compared and discussed. Electron microscopy observations revealed that morphology of the synthesized nanocrystals are quite different. The structures obtained using CVL are cubic in shape with about 1 μm lengths. Ablation process using Nd:YAG laser leads to structures which comprised of spherical, and platelet-like crystals. Sizes of the formed nanostructures in this case are in the range of 80-120 nm. The different results were attributed to the intrinsic difference of operating parameters of two employed lasers.

D. Pourmostafa et al [3], the effect of added MgO nanoparticles on nonlinear optical properties of 6CHBT liquid crystal doped with Sudan black B dye were studied by Z-scan

technique using of cw He-Ne laser at 632.8 nm. The cell used had homogeneous alignment. The MgO nanoparticles were added to 6CHBT liquid crystal doped with 0.3 wt% Sudan black B dye, at three concentrations of 0.1, 0.3 and 0.6 wt%. It was found that the added MgO nanoparticles did not significantly change the nonlinear refractive index of the compound at concentrations of 0.1 and 0.6 wt% while increasing it at 0.3 wt%. The reason for this different behavior and the increase in the nonlinear refractive index of the compound with a concentration of 0.3 wt% can be attributed to the accumulation of nanoparticles at high concentrations. This behaviour may be interpreted by dilution theory. As mentioned in Vafaee's work, MgO nanoparticles accumulate at concentrations higher than 0.5 wt% .The accumulation of nanoparticles within the composition reduces the number of single free nanoparticles and this may reduce their effect on nonlinear properties such as nonlinear refractive index. To add MgO nanoparticles to 6CHBT liquid crystal doped with Sudan black B dye also changed the sign of its nonlinear refractive index.

ShokuhiRad et al [4] In the present study, density functional theory calculations have been performed to explore the changes in the electronic properties of $Mg_{12}O_{12}$ nanocluster through exohedral doping with nickel. The changes in zero-point Energies (ΔZPE), thermal Energies (ΔE), thermal Enthalpies (ΔH), and thermal Free Energies (ΔG) of all positions are also calculated and compared with interaction energies. The HOMO-LUMO gaps of Ni-doped MgO nanocages are reduced significantly mainly due to the increase in the energies of HOMO. The Ni atom profoundly increases the polarizability (α) and first hyperpolarizability (βo) of MgO nanocluster however, a position dependent effect is observed. The value of α (and βo) changed from 219 (0.3) au for pristine MgO to 261 (1061), 263 (1122), and 262 (1240) au for positions P1, P2, and P3, respectively. These interesting results will be beneficial for the potential use of the MgO nanocluster in novel electronic and high-performance NLO materials.

Yuoraj S. Tamgadge et al [5], In this study, synthesis, structural, linear, and nonlinear optical properties of L-valine capped Zn doped MgO nanoparticles (NPs) are reported. L-valine capped (15 mol %) MgO NPs doped with Zn (1, 2, and 5 wt%) are obtained by chemical co-precipitation method and are calcined at 500°C for 2 h. X-ray diffraction (XRD) pattern shows major reflections at 2θ = 42.91°, 62.11°, and 78.34° corresponding to (200), (220), and (222) planes of MgO with a face-centered cubic structure, respectively, and the average particle size

is found to be 13 nm. Surface morphology is studied using HR-TEM and energy dispersive X-ray spectroscopy (EDS) attests the purity of prepared samples. Ultraviolet-visible (UV-vis) spectroscopic studies of both uncalcined and calcined samples attest the formation of NPs and strong blue shift in the excitonic absorption has been observed. Samples have been characterized for third-order nonlinear absorption using open aperture z-scan technique under continuous wave (CW) He-Ne laser and are found to exhibit strong nonlinear absorption coefficient due to thermal effect.

Marzieh-Nadafan et al [6], studied third-order optical nonlinearities of poly (ether) urethane open cell (PEUOC)/MgO nanocomposites, dissolved in dimethyl formamide are characterized by Z-scan technique with CW Nd:YAG laser at its second harmonic frequency of 532 nm with TEM00 Gaussian profile. The synthesized samples are also characterized by optical microscopy and scanning electron microscopy imaging. The nonlinear refractive indices and nonlinear absorption coefficients of the synthesized samples are obtained in the order of 10^{-8} cm^2/W with negative sign and 10^{-5} cm/W, respectively. The origin of optical nonlinearity in this case may be attributed due to the presence of strong saturable absorption effect. All the results suggest that the nonlinear coefficients of the synthesized samples can be controlled by nanoparticles content into PEUOC. Furthermore, the results show that PEUOC/MgO may be promising candidate for the application to optical limiting in the visible region.

C.S.K.Raju et al [7], The present study proclaims the importance of magnesium oxide nanoparticles in non-linear convective boundary flow over a radiated rotating disk with stretching in the radial direction. The flow governing equations are simplified to coupled non-linear ordinary differential equations (ODEs) by endeavoring von Karman transformations. The solution for the resulting system is obtained numerically by the help of Runge-Kutta and Newton's methods. The validity of the obtained numerical outcome is ensured by comparing with the existing literature as special cases. The comparative plots are provided for magnesium oxide + water and magnesium oxide + ethylene glycol nanofluid. Few of the several significant findings of the current study are: i) The time taken for execution is more in magnesium oxide with ethylene glycol mixture compared to magnesium oxide + water for all the considered non-dimensional parameters. This may be due to the ethylene glycol nanofluid is not amalgamated with magnesium oxide nanofluid properly when compared to water. ii) The nonlinear

convection parameter have higher heat transfer rate in ethylene glycol based magnesium oxide mixture when compared to water based magnesium oxide mixture due to nonlinear thermal variation in the flow.

Saeid Sahmani et al [8], fabricated hydroxyapatite (HA)-MgO scaffolds with the aid of the space holder technique using NaCl as the spacer type. After that, the fabricated samples are deposited in gelatin (GN) with ibuprofen (IBO) substitution to create GN-IBO thin surface coating. The samples are then synthesized chemically and the associated properties are studied using X-ray diffraction (XRD) and scan electron microscopy (SEM) equipped with the energy dispersive spectroscopy (EDS). The compressive strength, fracture toughness, hardness, porosity, bioactivity, degradation rate, wettability, and roughness of the manufactured HA-MgO bio-nanocomposite scaffolds containing different weight fractions of MgO nanoparticles are predicted. Accordingly, nonlinear mechanical behaviors including nonlinear free vibration and nonlinear vibrations associated with the prebuckling and postbuckling domains of an axially loaded plate-type bone implant made of the HA-MgO bio-nanocomposites coated with the GN-IBO thin layers are investigated analytically via a sandwich plate model. The obtained results reveal that magnesium has no considerable effect on the porosity; however it causes to enhance the compressive strength significantly. The presence of magnesium ions also leads to reduce the crystallinity of HA about 30–100 nm due to entering MgO nanoparticles into the network. The results related to the sample with 10 wt% MgO nanoparticles indicate that the microscopic structure of the fabricated bio-nanocomposite scaffold is three-dimensional with porous architecture. Also, it is shown that the solubility of the HA composed with MgO nanoparticles decreases with higher bioactivity.

CHAPTER 2

Materials and Methods

2.1 Synthesis

Nanostructures of pristine MgO and Co-doped MgO are synthesized using a modified auto combustion method. A stoichiometric amount of Magnesium nitrate hexahydrate (merk, 98% purity) and citric acid (merk, 98% purity) are taken as for the preparation of pristine MgO and Magnesium nitrate hexahydrate, citric acid, and Cobalt nitrate hexahydrate for (x= 0, 0.01, 0.03, 0.05) nanostructures. The mixture is dissolved in deionized water wherein citric acid is used as a fuel. 30 ml of nitric acid is added to the above solution. A solution with no precipitation and sedimentation is obtained after 30 minutes of stirring. Ammonia is added to maintain the pH as neutral. The solution is heated on a hot plate at about 250 ºC in the combustion chamber. On the completion of dehydration, internal combustion starts, and a black coloured powder is obtained. The resultant powder is heated to about 600 ºC for 3 hrs in the high-temperature furnace to remove impurities. The sintered samples are taken for different characterizations.

2.2 Characterization Techniques

2.2.1 X-Ray Diffraction

X-ray diffraction is one of the extensive analytical instruments to detect the polymorphism and crystal structure. Crystals are symmetrical arrays of atoms containing rows and planes of high packing density, so they are able to be three-dimensional diffraction gratings. When X-rays of a given frequency strike an atom, they interact with its electrons, causing them to vibrate with the frequency of the X-ray beam. When the regular interval spaced atoms are irradiated by a beam of X-rays, the scattered radiation undergoes interference. In certain direction, the constructive interference occurs and destructive interference appears in other directions. When an electron strikes a metal target at high speed, the electrons of the target are excited to raise a shell of higher energy level and the outer electrons fall to fill in the vacancy, X-ray are emitted then. K X-rays are emitted by an electron from the L to the K shell and K X-rays are produced by an electron from M to K shell. The K X-ray is used for the characterization analysis. Each crystalline plane reflects a part of X-ray beam and also permits part of it to pass through. When

X-rays strike a crystal, the beam is not only from the surface layer of atoms, but also from atoms underneath the surface to a considerable depth. In fact, the beam would be reflected not from just two lattice planes, but from a large number of parallel planes. The spacing (or distance) between planes is represented by the symbol d. The crystalline size "**d**" can be evaluated from the full-width at half-maximum (FWHM) value of the reflections of the films, using the Scherer equation

$$D= 0.9\lambda/(\beta \cos\theta)$$

where is the broadening of the diffraction line measured at half its maximum intensity in radians and is the wavelength of the X-rays . The lattice parameters of the powders can be calculated according to Bragg's law. The Bragg s law states that the path difference between the beams scattered by the lattice planes should be an integral multiple of the wavelength and mathematically is represented as follows,

$$n\lambda= 2d \sin\theta$$

n = is an integer indicating the order of diffraction (n = 1, 2, 3…)

λ= wavelength of the incident X-rays (nm)

d = interplanar distance in nm (hkl)

θ= angle of incidence or refection of X-ray beam

When the relationship is satisfied, the reflected rays will be in-phase and constructive interference will result. X-ray diffractometry is a powerful instrument to apply in the determination of crystal structure, lattice parameters, crystal orientation (degree of texture), crystal size, crystallinity, phase composition, residual stress and orientation relationships. The 2θ values obtained from the position of the Bragg peaks from XRD pattern are used to obtain the inter planar spacing. In case of cubic lattice the inter planar distance d (hkl) is related to the unit cell dimension in the following manner

$$d_{hkl} = \frac{a}{h2+k2+l2}$$

d_{hkl} = is the interplanar distance for hkl planes

a – is the unit cell dimension and(hkl) – are Miller (reflections) indices of crystal phase.

2.2.1.1 Instrumentation

X -ray diffractometer consist of three basic elements

1 .An X - ray tube

2. An X - ray detector

3. A sample hold

X - rays are generated in the cathode ray tube by heating a filament to produce electrons, accelerating the electrons towards a target by applying a voltage , and bombarding the target material with electrons. When electrons have sufficient energy to dislodge inner shell electrons of the target material, characteristic X-ray spectra are produced .These spectra consist of several components, the most common being K_α, K_β.

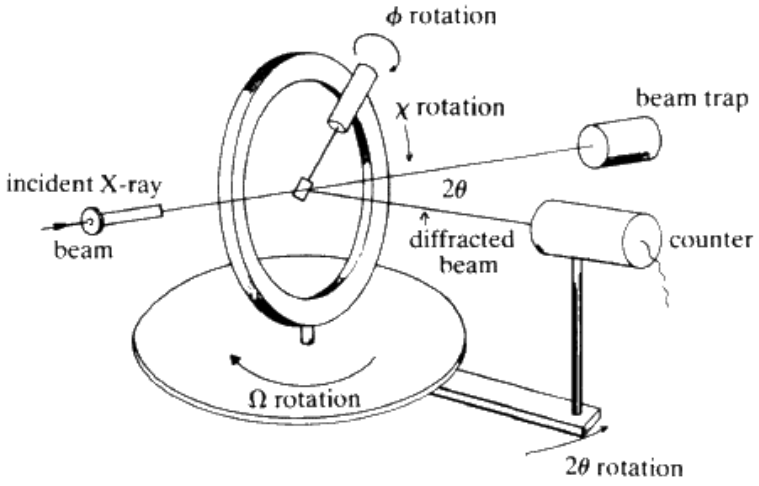

Fig: 2.1 XRD instrumentation

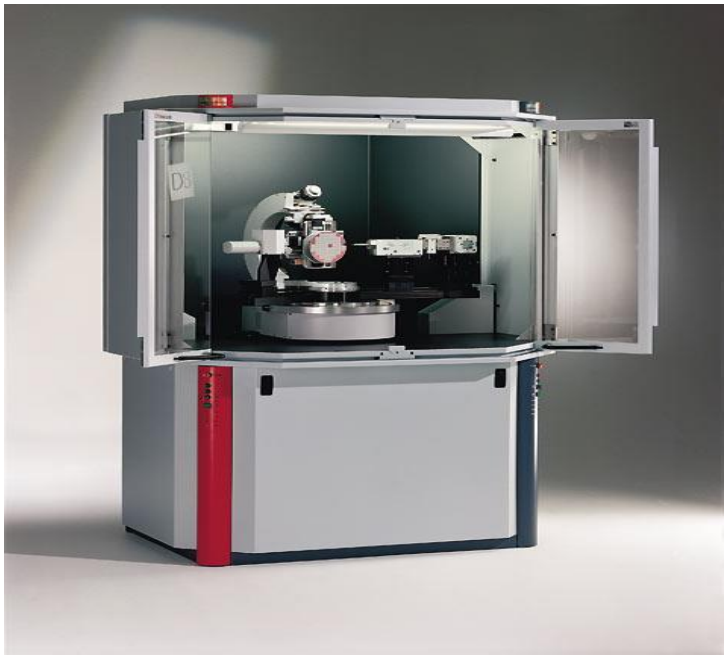

Fig: 2.2 XRD diffractometer

The most commonly used X-ray instrument is the powder diffractometer. It has a scintillation or GEiger counter. The detector shows a range of scattering angles. The values odd can be calculated from the graph. A set of peaks and their heights is adequate for phase identification.

2.2.2 UV- Visible spectroscopy

A more reliable way than PL to study the fundamental band gap is optical absorption. Absorption is the direct measurement of photo-excitation across the band gap. This refers to absorption spectroscopy or reflection spectroscopy in the ultraviolet visible spectral region. This means it uses light in the visible and adjacent ranges (near UV and near IR).The absorption or reflectance in the visible range directly affects the perceived color.

2.2.2.1 Working Principle: Molecules containing π electrons or nonbonding electrons can absorb the form of ultra violet or visible light to excite these electrons to higher antibonding molecular orbitals. The more easily excited electrons longer the wavelength of light it can absorb.

2.2.2.2 The Beer –Lambert law: It states that absorbance of a solution is directly proportional to the concentration of absorbing species in the solution and path length. Thus for

a fixed path length UV/Vis spectroscopy can be used to determine concentration of absorber in the solution. The method is most often used in a quantitative way to determine concentrations of absorbing species in solution using Beer – Lambert law

$$A = \log 1_0(I_0 / I) = €CL$$

A – Absorbance,

I_0 – intensity of incident light at given wavelength,

I – transmitted intensity,

L – Path length through sample,

C – Concentration of absorbing species,

€ - Molar absorptivity.

UV/VIS spectrometer measures the intensity of light passing through a sample (I) and compares it to intensity of light before it passes through sample (I_0). The ratio I/I_0 is called transmittance and usually expressed as a percentage (%T). The absorbance A is based on the transmittance.

$$A = - \log (\%T/ 100\%)$$

The UV-Visible spectrometer can also be configured to measure reflectance. In this case the spectrophotometer measure the intensity of light reflected from a sample (I) and compares the intensity of light reflected from reference material (I_0). The ratio I/I_0 is called reflectance and usually expressed as percentage reflectance (%R).

2.2.2.3 Tauc Plot

In an absorption measurement, a beam of monochromatic light with tunable wavelength is shined on a sample, while the intensity of the transmitted light is detected on the backside of the sample. When the photon energy is higher than the band gap of the material, absorption of the photons can take place and electrons can be raised in energy from the valence band to the conduction band creating electron hole pairs. If one plots the square of the absorption coefficient as a function of photon energy, the interband excitation appears as a linear absorption edge. The band gap energy can be determined from the intercept of the absorption edge and the base line. The material absorbs less and can transmit the photons having energy less than the band gap of the semiconductors, as the energy is insufficient to create an electron

hole pair. The ability of a material to absorb photons of a given wavelength is measured quantitatively by the optical absorption coefficient (α), measured in units of reciprocal distance. There are two major types of intrinsic absorption processes involved in determining they are the direct and indirect absorption. As a general rule, the larger the band gap, the smaller is the value of $\alpha$for a given wavelength but absorption coefficient also depends on the density of states in the conduction and valence bands. The optical absorption coefficient a is related to the energy band gap and it is given by the following equation

$$\alpha\nu h=B(\nu h-E_g)^n$$

where B is a constant, Eg is an optical band gap and n is the exponent. For crystalline semiconductors, n is 1/2, 3/2, 2 and 3 when the transition is direct allowed, direct forbidden, indirect allowed and indirect forbidden, respectively. Apparently the plot of $(\alpha\nu h)^2$ or $(\alpha\nu h)^{1/2}$ against (νh) provides the nature and Eg value of a particular film, and is called Tauc's plot. The direct optical absorption is a first-order process involving only the absorbed photon and can be represented approximately as a vertical line on the energy versus wave vector plot. The absorption transition conserves energy so that E = h ν (where h is the photon energy) and there is no change in wave vector (k) between initial and final states except for the small momentum of the photon. An indirect optical transition is a second order process involving both the absorbed photon and simultaneously absorbed or emitted phonon, which occurs when the minimum of the conduction band and the maximum of the valence band occur at different values of the wave vector k. Here the absorption transition conserves energy by requiring Δ E = h + E_p, where E_p is the photon energy and the change in k between the initial and final states k is just equal to the value of k of the phonon involved. The type of spectrophotometer features a continuous change in wavelength and an automatic comparison of light intensities of sample and reference material. The ratio of the latter is the transmittance of the sample, which is plotted as a function of wavelength. The automatic operation eliminates many time-consuming adjustments and provides a rapid spectrogram. In the double beam-in-time arrangement, energy from a dispersed source passes through the exit slit of the monochromator and is alternated between reference and sample compartments at a rate of 60 Hz (or other fixed frequency). These two beams alternately strike a single detector where their optical energy is converted to an electrical signal. The output of the detector is an alternating signal whose amplitude is proportional to the difference in intensities in the two channels. The reference

signal is maintained constantly by an automatic slit servo system, which widens or closes the slits to achieve a 100% transmittance baseline. The switching between reference and sample paths is done by a rotating half-sector mirror system, or by a vibrating mirror assembly, or by a stack of thin horizontal glass plates that are silvered along their edges and alternately oriented, or by a prismatic beam splitter.

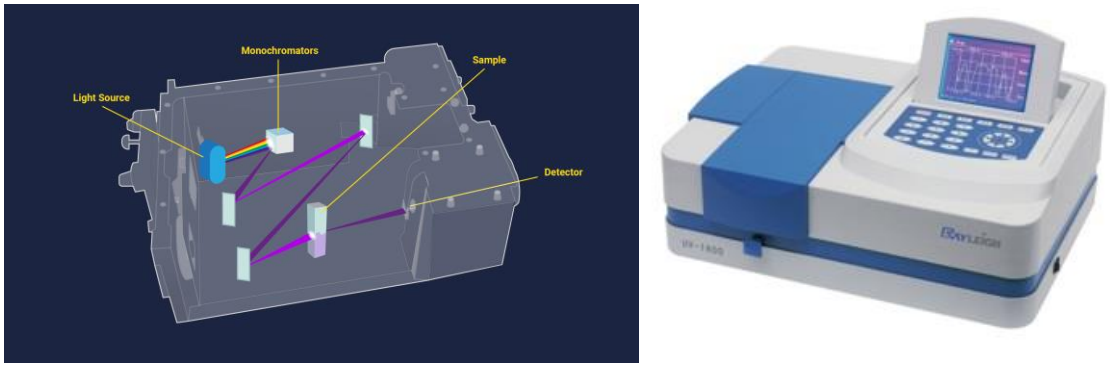

Fig.2.3 UV-Visible spectrophotometer

2.2.3 Field Emission Scanning Electron Microscopy

The scanning electron microscopy is one of the powerful techniques used to analyze the microstructure in sample. The scanning electron microscopy (SEM) was first developed by Von Avdenne and is used for determination of the grain size, porosity, grain boundary, inclusion.

Fig.2.4 Field Emission Scanning Electron Microscope

The intrinsic properties such as magnetic, Curie temperature and anisotropy depend on chemical composition, electronic structure of magnetic ions and crystal chemistry. However, the properties like permeability, coercity are strongly dependent on grain size, porosity, and inclusion. The structure with large crystallites favors domain wall motion with high permeability and low coercivity. Fine grain structure shows the wall and results in the large retentivity and coercivity. The proper grain orientation favors maximum BH value. The grain boundaries act as a source of impurities and usually prefer sites for inclusions. The decreasing grain size enhances the porosity and decreases the conductivity. The firing temperature influences grain size and porosity. The high permeability values are related with the large crystallites without pores or imperfection and small anisotropy. SEM makes use of an electron beam to form an image of specimen. Its magnification is very high up to 300000 times and above. This technique unable high magnification, large depth of field, greater resolution and provides chemical composition and crystallographic information. The SEM makes use of an electron beam generated as result of impact of fine beam against specimen. By modulation of brightness of a synchronized CRT or computer monitor by any one of signals generated images of specimen surface can be obtained. The microscope consists of

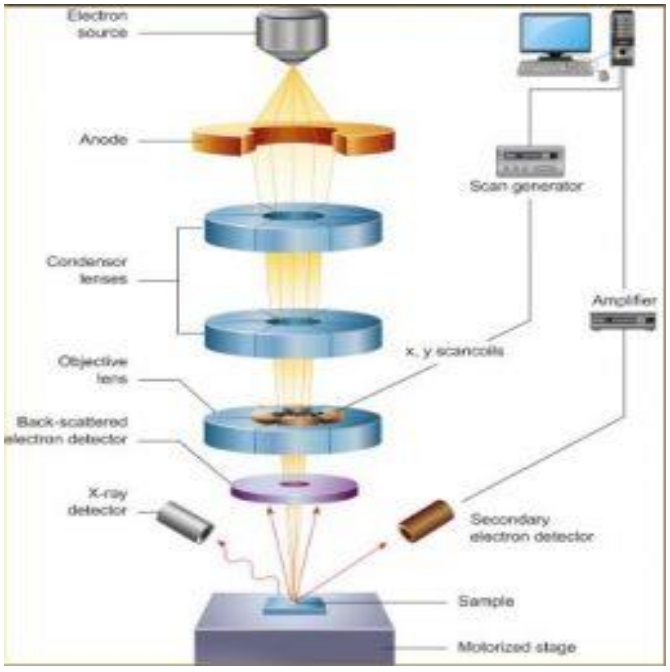

Fig.2.5 Components of SEM

1) An arrangement for the production of a fine electron beam; a few ten or thousands of A_0 units in diameter.
2) Electromagnetic lenses
3) An arrangement to scan the probe across the object.

According to the basic principle of scanning electron microscopy, a signal varying with time and position is obtained by collecting the secondary electrons. The signal is amplified and the reconstituted image is recorded on the enlarged scale.

Magnification is given by ratio of length L of scan on CRT to the length of scan X on specimen.

For 10 cm^2 CRT screen, Magnification M = 10/X cm.

If X = 10 micron magnification is 10000

X = 2 micron magnification is 50000

X = 1nm magnification is 500000.

SEM has ability to reveal shape, size and distribution of inclusions and second phase network. The presence of magnetic domains in a ferromagnetic specimen can be imaged.

2.2.4 Energy Dispersive Spectroscopy (EDS)

Fig: 2.6 Instrumental setup of EDS

Energy dispersive X-ray spectroscopy (EDS or EDX) is a compositional microanalysis technique used in conjunction with transmission electron microscopy (TEM) in which features

as small as 1 m can be analyzed. EDS detects the characteristic X-rays emitted from the sample during bombardment by an electron beam, to characterize the elemental composition of the analyzed volume. When the sample is bombarded by the electron beam, X-ray photons, which are produced by transitions between deep atomic levels, are ejected from the atoms comprising the sample's surface. The X-ray energy is the characteristic of the element from which it was emitted. When an X-ray strikes the EDS detector, it creates a charge pulse that is proportional to the energy of the X-ray. The charge pulse is converted to a voltage pulse (which remains proportional to the X-ray energy) by a charge-sensitive preamplifier. The signal is then sent to a multichannel analyzer where the pulses are sorted by voltage. The spectrum of X-ray energy versus counts is evaluated to determine relative abundance of emitted X-rays versus their energy and hence the elemental composition of the sample is evaluated.

2.2.4.1 Qualitative analysis: X-ray transition energy derived from the EDS spectrum of the sample can be compared with known characteristic X-ray energy values for determining the presence of an element in the sample. Elements with atomic numbers ranging from that of beryllium to uranium can be detected. The minimum detection limits vary from approximately 0.1 to a few atomic percent, depending on the element and the sample matrix.

2.2.4.2 Quantitative analysis: Quantitative results can be obtained from the relative X-ray counts at the characteristic energy levels for the constituents of the sample. Semi quantitative results are readily available without standards by using mathematical corrections based on the analysis parameters and the sample composition. The accuracy of non-standard analysis depends on the sample composition. Greater accuracy is obtained using known standards with structure and composition similar to that of the unknown sample.

2.2.4.3 Elemental mapping: Characteristic X-ray intensity can be measured relative to lateral position on the sample. Variations in X-ray intensity at any characteristic energy value indicate the relative concentration of the applicable element across the surface. One or more maps are recorded simultaneously using image brightness intensity as a function of the local relative concentration of the element(s) present. About 1 m lateral resolution is possible.

2.2.4.4 Line profile analysis: The TEM electron beam can be scanned along a preselected line across the sample while X-rays are detected for discrete positions along the line. Analysis

of the X-ray energy spectrum of each position provides plots of the relative elemental concentration for each element versus position along the line.

2.2.5 Third Order Nonlinearity Studies

2.2.5.1 The Z - Scan Technique

The Z – scan technique is method which can measure Nonlinear Absorption (NLA) and Nonlinear Reflection (NLR) in solids, liquids and liquid solutions. This is standard technique for separately determining the nonlinear changes in index and changes in absorption. A series of Z scans at varying pulse widths, frequencies; focal geometries etc. along with a variety of experiments are often needed.

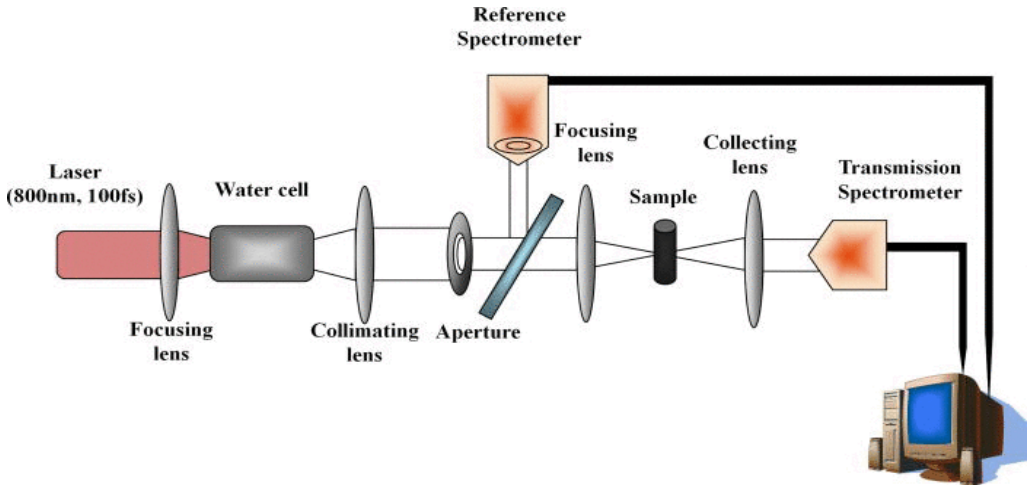

Fig: 2.7 Experimental setup of Z-scan

2.2.5.2.Nonlinear Absorption

Then nonlinear absorption can be determined using two parameter fit to close aperture Z-scan, the normalized change in transmitted energy

$\Delta T(Z) \approx - q0 / 2\sqrt{2}\Delta T(Z) \cong -q_0/(2\sqrt{2})1/[1 + Z^2/ Z_0^2$,

Furthermore, q0 is defined as

$$q_0 = \beta I L_{eff} / (1 + z^2 / z^2_0)$$

z_0 is defined as the diffraction length, the laser intensity at the focal point is denoted as I, and the effective thickness of the sample is L_{eff}, which is calculated as

$$L_{eff} = (1 - e^{-\alpha l})/\alpha$$

Here, l is the thickness of the Z-scan experiment cell, and α is the linear absorption coefficient of the sample that can be calculated from UV-Vis analysis by using the Beer–Lambert law as follows:

$$\alpha = 2.303A/t$$

where A is the absorbance of the sample at 532 nm and t is the thickness of the cell in a UV-Vis spectroscopy device. By fitting the open-aperture Z-scan data, it is possible to calculate NLO absorption coefficients. From the value of β, the imaginary part of susceptibility can be calculated through the following formula:

$$Im\chi 3(esu) = (10^{-2}\varepsilon_0 c^2 n^2_0 \lambda/4\pi^2)\beta(cm/W)$$

where λ is the excitation wavelength, n_0 is the linear refractive index of the sample, ε_0 is the permittivity of free space, and c is the velocity of light in a vacuum.

2.2.5.3. Nonlinear Refraction

The change in transmittance between peak and valley in a Z-scan is

$$\Delta T_{pv} = T_p - T_v$$

Where T_p and T_v are peak valley transmittances. The empirically determined relation between the induced phase distortion $\Delta\phi_0$ and ΔTpv for third order nonlinear refractive process in absence of nonlinear absorption is

$$\Delta Tpv \approx 0.406(1 - S)^{0.27}|\Delta\phi_0|$$

$\Delta\varphi 0$ is the on-axis phase shift that is related to n_2 as

$$\Delta\varphi_0 = 2\pi n_2 I L_{eff}/\lambda$$

In this formula, λ is the wavelength of the incident laser beam, I is the laser intensity at the focal point, and L_{eff} is the effective thickness of the sample. The NLO refractive indices of the material can be calculated by fitting standard equations with the experimental data. The nonlinear refractive index coefficient n_2 is proportional to the real part of χ3 as

$$\mathrm{Re}\chi 3(\mathrm{esu}) = (10^{-4}\varepsilon_0 c^2 n^2{}_0/\pi)n2(\mathrm{cm}^2/\mathrm{W}$$

where c is the light velocity in a vacuum and ε_0 is the vacuum permittivity. The third-order optical nonlinearities $\chi 3$ are calculated as follows:

$$\left|\chi^{(3)}\right| = \left[Re\,\chi^{(3)^2} + Im\,\chi^{(3)^2}\right]^{\frac{1}{2}}$$

Chapter -3

Results and Discussion

3.1 X-Ray Diffraction Analysis

X-ray diffraction technique was used to analyse phase purity, crystallinity as well as crystal structure of prepared sample. The XRD pattern were indexed and all the peaks were well matched with the cubic structure of MgO using the standard date [JCPDS - card no 74-1225] without any other impurity phase other than dopants concentrations and having the space group *fm-3 m*. XRD pattern of MgO, $Mg_{0.99}Co_{0.01}O$, $Mg_{0.97}Co_{0.03}O$, $Mg_{0.95}Co_{0.05}O$ was recorded in 2θ range shown in **Fig 3.1** peaks were observed at 37.54^0, 42.79^0, 62.01^0,74.57^0 and 78.28^0 which corresponds to plane (1 1 1), (2 0 0), (2 2 0), (3 1 1) and (2 2 2). The lattice constants, lattice volume and crystallite size of $Mg_{(1-x)}Co_xO$ $(x = 0, 0.01, 0.03, 0.05)$ are assembled in the **Table 3.1** .From the **Table 3.1** the crystallite size increases as the concentration of dopants increases and also the peaks becomes sharper .The crystalline size of the MgO and Co doped MgO nanoparticles has been estimated by using the Debye-Scherrer relation

$$D = \frac{K\lambda}{\beta Cos\theta}$$

where D is the crystallite size, is a constant taken to be 0.94, λ is the wave length of X-rays,β is the full width at half maximum intensity and θ is the Bragg's angle (angle of diffraction).

Table 3.1 Lattice parameters and crystallite size of $Mg_{(1-x)}Co_xO$ $(x = 0, 0.01, 0.03, 0.05)$

Sample code	a(Å)	b(Å)	c(Å)	V (Å^3)	α = β = γ (°)	Crystallite Size (nm)
MgO	**4.2260**	**4.2260**	**4.2260**	**75.4717**	**90**	**10.62**
$Mg_{0.99}Co_{0.01}O$	**4.2232**	**4.2232**	**4.2232**	**75.3249**	**90**	**12.48**
$Mg_{0.97}Co_{0.03}O$	**4.2173**	**4.2173**	**4.2173**	**75.0099**	**90**	**13.19**
$Mg_{0.95}Co_{0.05}O$	**4.2134**	**4.2134**	**4.2134**	**74.7992**	**90**	**13.52**

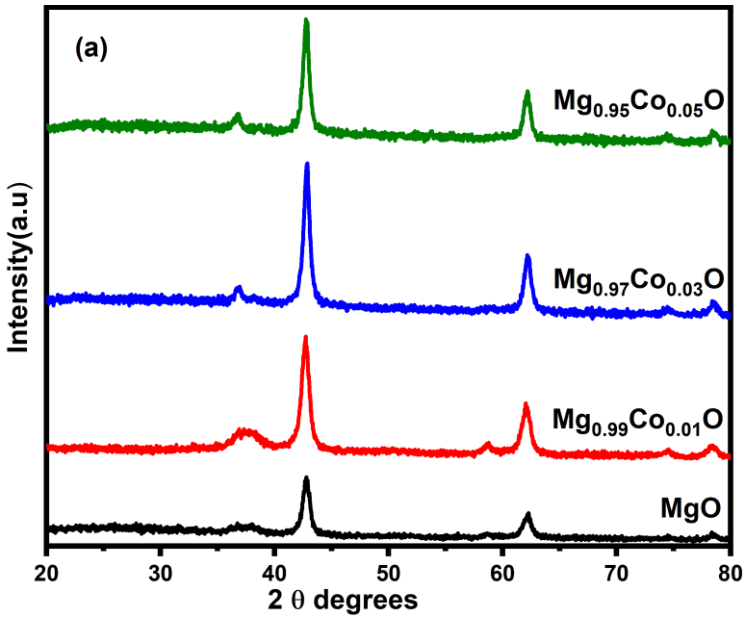

Fig 3.1 XRD profile of $Mg_{(1-x)}Co_xO$ $(x = 0, 0.01, 0.03, 0.05)$

3.2 Rietveld Refinement

Fig. 3.2 shows the rietveld refinement of $Mg_{(1-x)}Co_xO$ $(x = 0, 0.01, 0.03, 0.05)$ and **Table 3.2** summarizes the determined parameters obtained from the refinement. The results clearly depict the absence of any additional peaks in the framework of both pristine and doped MgO.

Table.3.2. Refined parameters of $Mg_{(1-x)}Co_xO$ (x= 0, 0.01, 0.03, 0.05)

Sample	R_p	R_{wp}	R_e	χ^2
MgO	**71.2**	**37.8**	**22.6**	**2.80**
$Mg_{0.99}Co_{0.01}O$	**44.7**	**28.8**	**14.75**	**3.83**
$Mg_{0.97}Co_{0.03}O$	**52.4**	**27.5**	**16.00**	**2.95**
$Mg_{0.95}Co_{0.05}O$	**74.1**	**32.2**	**19.18**	**2.82**

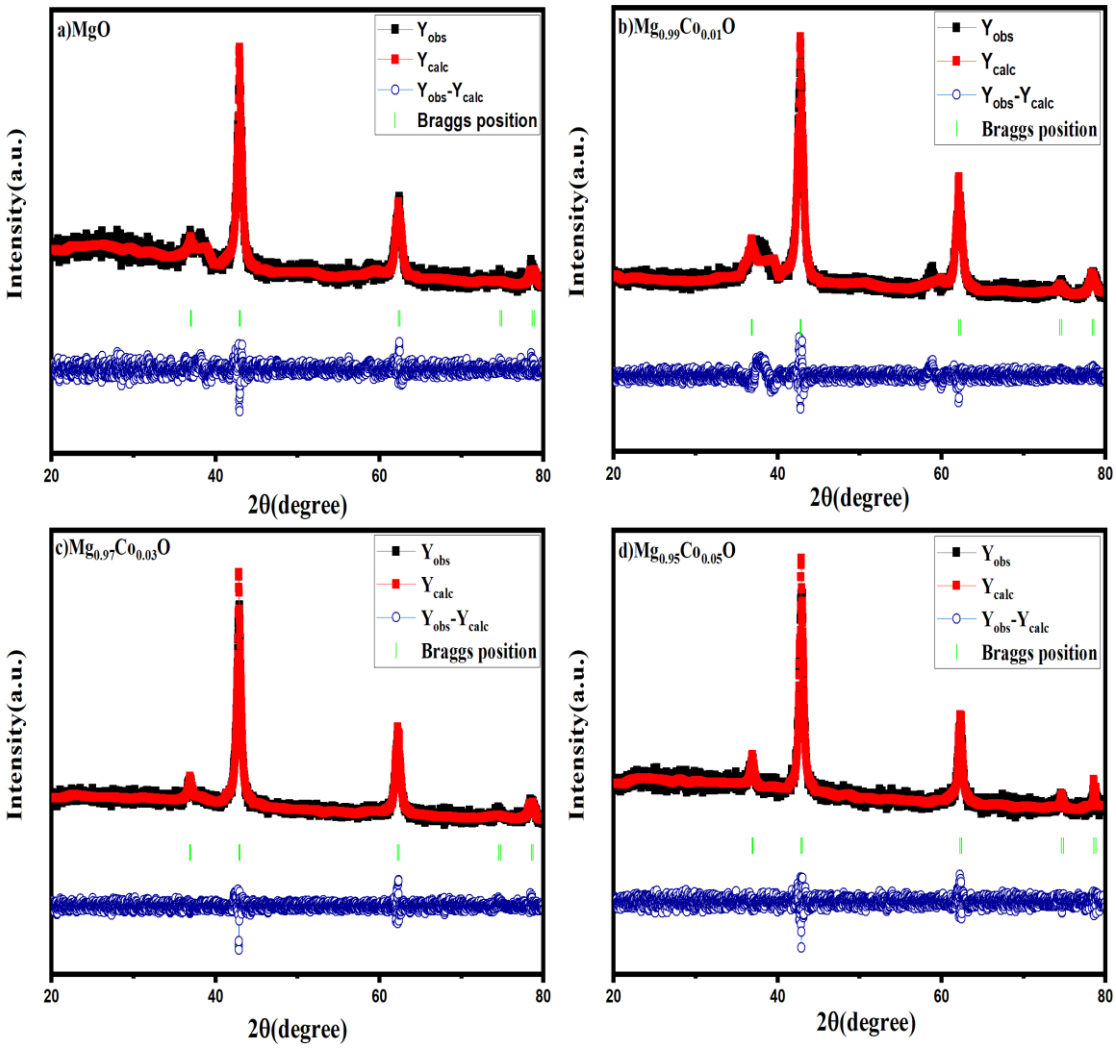

Fig. 3.2 Rietveld refinement profile of $Mg_{(1-x)}Co_xO$ $(x = 0, 0.01, 0.03, 0.05)$

3.3 Field Emission Scanning Electron Microscopy (FESEM)

Fig.3.3 indicates the FESEM image of $Mg_{(1-x)}Co_xO$ $(x = 0, 0.01, 0.03, 0.05)$ from which the surface morphology can be determined. From the FESEM analysis, it is found that MgO nanoparticles have a flower petal like morphology. There could be the presence of voids and pores. Also large amount of gases were seen to escape out of the reaction mixture during combustion.

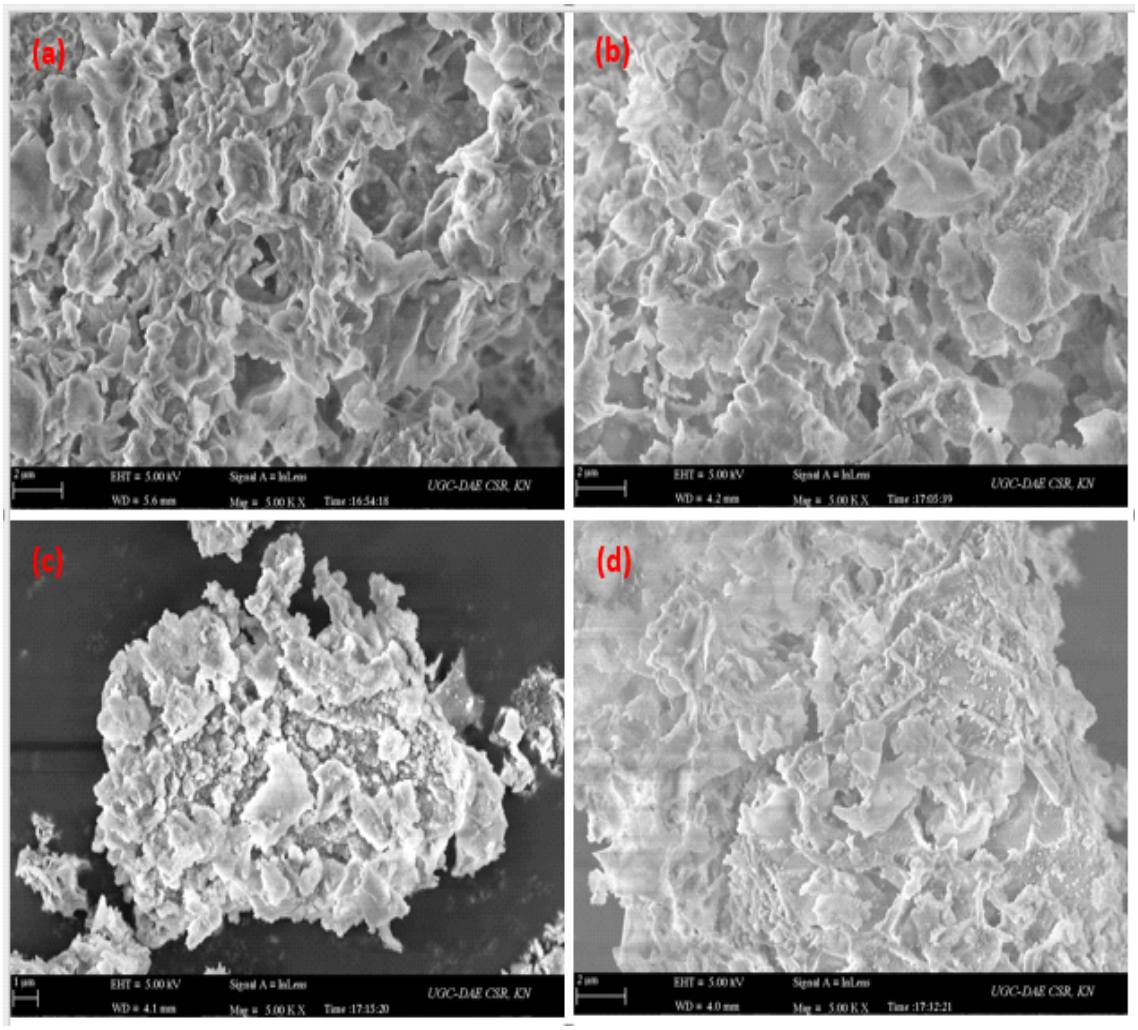

Fig. 3.3 FESEM image of $Mg_{(1-x)}Co_xO$ $(x = 0, 0.01, 0.03, 0.05)$

3.4 Energy Dispersive Spectroscopy (EDS)

EDS spectra of $Mg_{(1-x)}Co_xO$ $(x = 0, 0.01, 0.03, 0.05)$ are given in **Fig 3.4.** Chemical composition of the nanostructures is evaluated by using energy dispersive spectral mapping**.** Spectrum confirms the presence of Magnesium, Oxygen for pristine MgO and Magnesium, cobalt, oxygen for doped samples. Absence of foreign elements shows the phase integrity of the nano-sized structures. The increase in the percentage of Co indicates the substitution of oxygen by cobalt. The presence of carbon observed in the EDX spectrum could be from the carbon tape used for the measurements, not from the nanostructures.

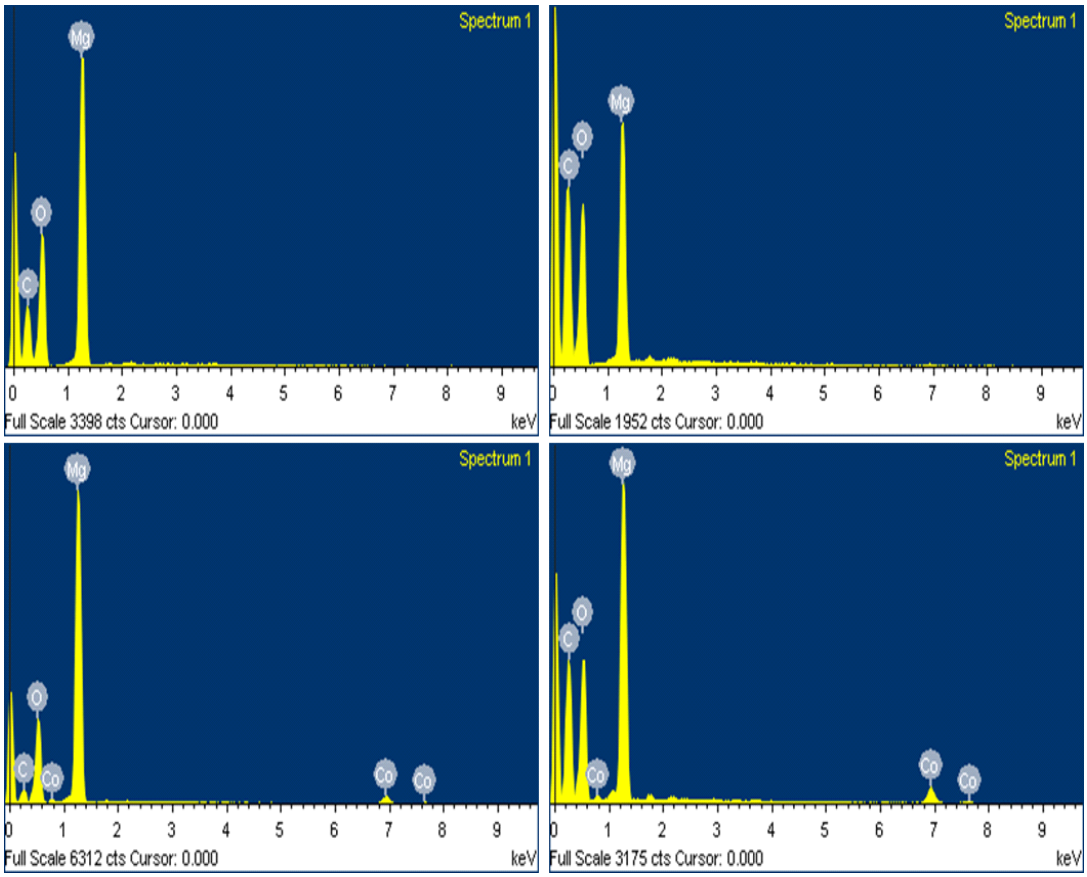

Fig. 3.4 EDS spectra of $Mg_{(1-x)}Co_xO$ $(x = 0, 0.01, 0.03, 0.05)$

3.5 Linear Optical studies

Linear optical behaviour of synthesized pristine and doped nanostructures can be identified from the UV-Visible absorbance spectrum, from which the classification of electronic transition along with bandgap energy can be evaluated. Whenever a semiconductor absorbs incident energy greater than its bandgap energy (E_g), the electron from its valence band will shift towards the conduction band and this causes an abrupt increase in the absorbance. Generally, the type of transition depends on absorption coefficient (α) and photon energy. If the momentum of electron is conserved for a transition, then it is said to be as direct transition and on the other hand if the momentum of electron is not conserved, then it is called as indirect transition.

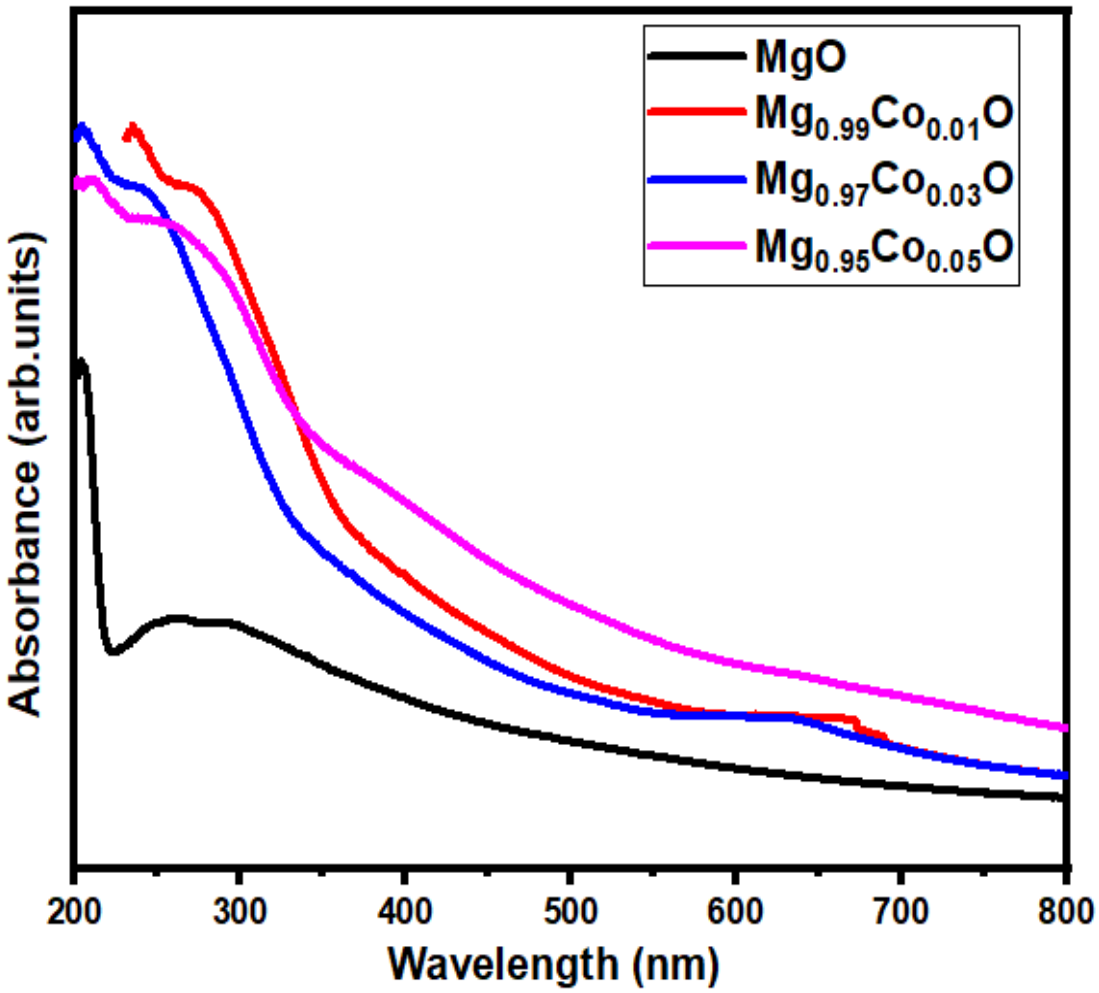

Fig.3.5 Absorbance spectra of $Mg_{(1-x)}Co_xO$ $(x = 0, 0.01, 0.03, 0.05)$

Fig 3.5 gives the absorbance spectra of $Mg_{(1-x)}Co_xO$ $(x = 0, 0.01, 0.03, 0.05)$. A broad absorption peak in spectrum located at ~230 nm for all samples.

For direct band gap materials, like MgO, bandgap (E_g) are related by the Tauc relation:

$$(\alpha h\upsilon)^{1/n} = A(h\upsilon - E_g)$$

where $E_g$stands for the energy bandgap and n denotes the kind of optical transition, here it is ½.

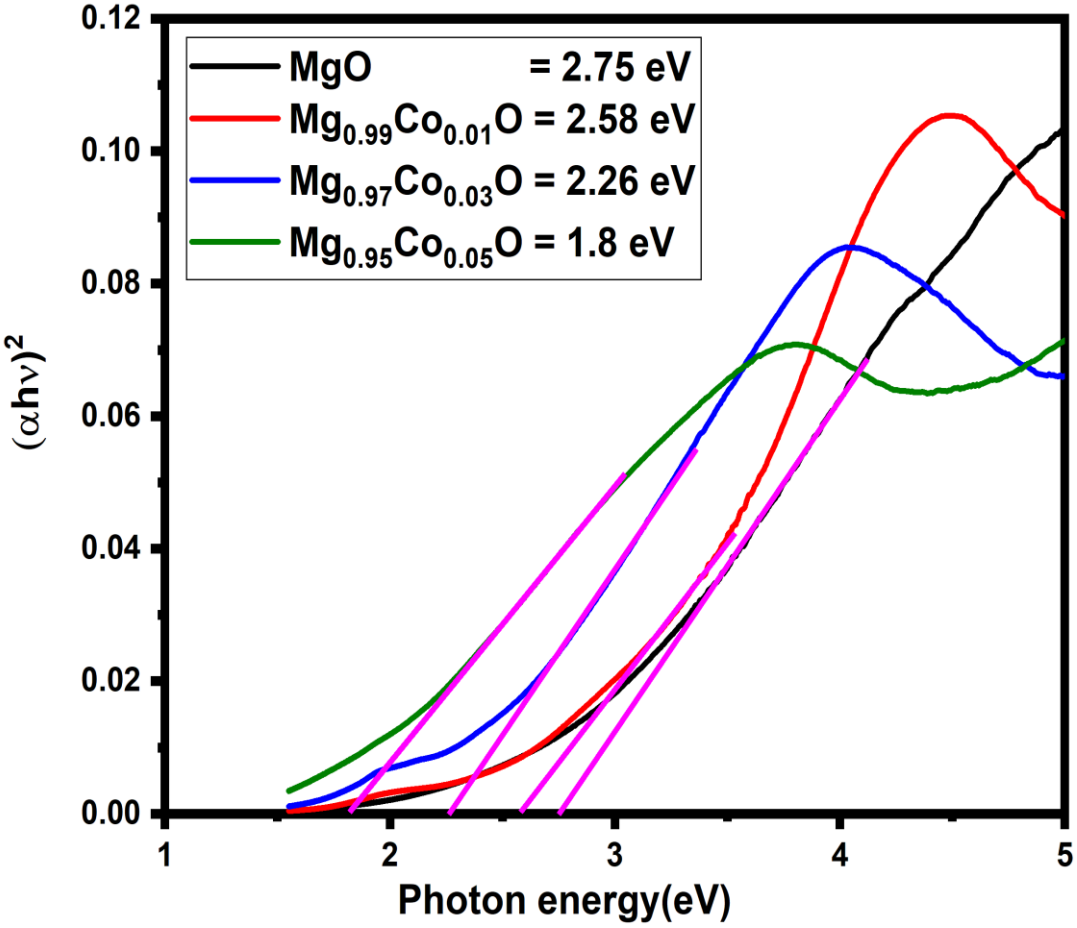

Fig. 3.6 Bandgap of $Mg_{(1-x)}Co_xO$ $(x = 0, 0.01, 0.03, 0.05)$

The bandgap energy has been evaluated by plotting $(\alpha hv)^2$ and photon energy along Y and X-axis respectively is given in **Fig.3.6**. By extrapolating the linear section in **Fig. 3.6,** energy bandgap of pristine and doped nanostructures can be calculated. From the bandgap calculations, it is found that the bandgap is decreasing, which confirms the formation of intra-band level in the bandgap. Hence bandgap narrowing is confirmed in cobalt doped MgO. The presence of dopants/chemical defects or surface oxygen vacancies in the bandgap leads to the decrease in the bandgap.

3.6 Nonlinear Optical studies- under continuous wave laser

3.6.1 Open aperture Z-scan method

The third order (NLO) properties like nonlinear absorption (NLA) and nonlinear refractive

index (n_2) were determined by simple and accurate Z-scan technique mentioned by Sheik Bahae et al.[1]. The NLO measurements of pristine and Ni doped copper oxide nanostructures were examined using a continuous wave diode pumped solid state laser (CW-DPSS) with 532 nm wavelength as excitation source having an output power about 100 mW. All the prepared samples were dispersed in an appropriate amount of ethylene glycol because it provides high stability to the sample for Z-scan measurements due to its highly viscous nature. Also this solvent does not possess any nonlinearity under laser irradiation [2].

The intensity dependent nonlinear absorption and refraction are expressed by the equations [3].

$$\alpha\,(I) = \alpha + \beta_{eff}$$

$$n\,(I) = n_0 + n_2 I$$

where α denotes the linear absorption coefficient, n_0, the linear refractive index, β_{eff} the nonlinear absorption coefficient, n_2 the nonlinear refractive index and I the intensity of the laser beam.

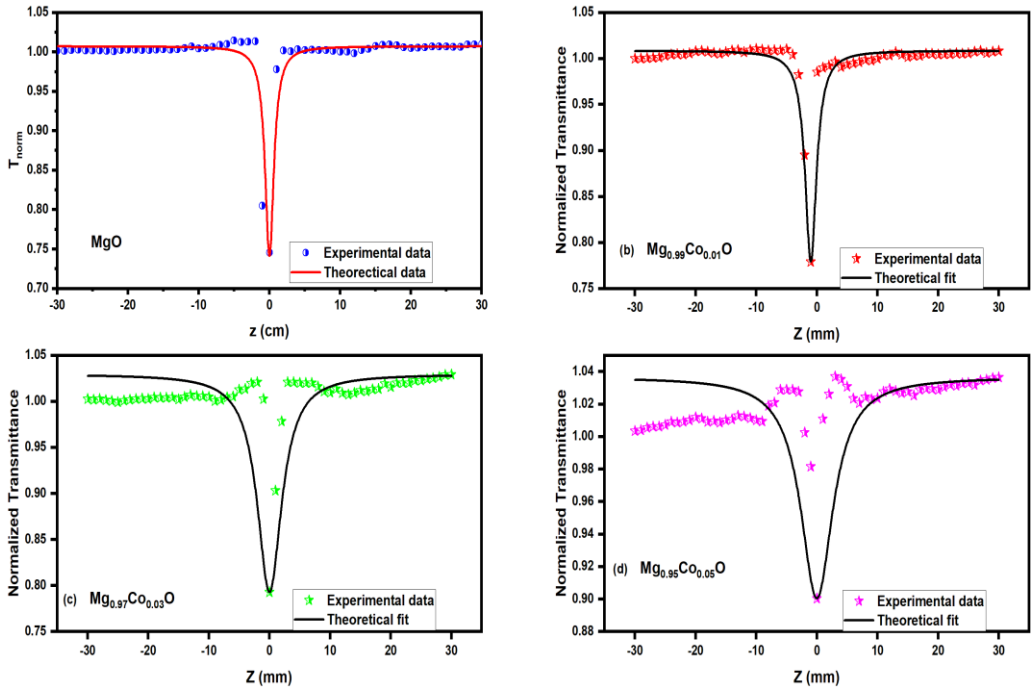

Fig. 3.7 Open aperture Z-scan data of $Mg_{(1-x)}Co_xO$ $(x = 0, 0.01, 0.03, 0.05)$

Fig. 3.7 shows the nonlinear absorption coefficient (NLC) of $Mg_{(1-x)}Co_xO$ $(x =$

$0, 0.01, 0.03, 0.05$)obtained from open aperture Z-scan cures. For all samples, there is dip in transmittance value at focus (z=0). This valley like pattern represents reverse saturation absorption (RSA) behavior. Generally, mechanism responsible for RSA can result from different processes including two photon absorption (2PA), free carrier absorption (FCA), excited state absorption (ESA), nonlinear scattering [4]. The valley like curve reveals that all the synthesized samples exhibit nonlinear absorption, whereas the maximum transmittance at the focus is due to RSA behaviour. In addition to the valley, a peak is also observed at the focus (z = 0) for all nanostructures, indicating saturable absorption (SA).Whereas a small hump on both sides of focus is observed for Co doped MgO, as the sample approaches the focus, the transmittance increases and depicts SA behavior; as it reaches the focus, the transmittance decreases and forms a valley, indicating RSA behavior. Again, when the sample is translated further away from the focus, the transmittance increases, denoting a SA behavior. The normalized transmittance for the open aperture condition is given by

$$T(z, S = 1) = \sum_{m=0}^{\infty} \frac{[-q_0(z)]^m}{(m+1)^{\frac{3}{2}}}$$

For $q_0(0) < 1$, (0) < 1, where $q_0(z) = \frac{\beta_{eff} I_0 L_{eff}}{(1+ {z^2}/{z_R^2})}, z_R = \frac{k\omega_0^2}{2}$, where is the diffraction length of the beam .The experimental measurements of and allow one to determine the real and imaginary parts of the third-order nonlinear optical susceptibility according to the following relations [5].

$$Re\ \chi^{(3)}(esu) = 10^{-4} \frac{\varepsilon_0 C^2 n_0^2}{\pi} n_2 \frac{cm^2}{W}$$

Where ε_0 is the vacuum permittivity, and C the light velocity in vacuum:

$$Im\ \chi^{(3)}(esu) = 10^{-2} \frac{\varepsilon_0 \lambda C^2 n_0^2}{4\pi^2} \beta_{eff} \frac{cm^2}{W}$$

The absolute value of $\chi^{(3)}$ is calculated from

$$|\chi^{(3)}| = \left[Re\ \chi^{(3)^2} + Im\ \chi^{(3)^2}\right]^{\frac{1}{2}}$$

3.6.2 Closed aperture Z-scan method

Closed aperture Z-scan experiments are performed to investigate the nonlinear refraction behaviour of the nanostructures, as demonstrated in **Fig .3.8**. The absence of aperture provides the nonlinear absorption coefficients, whereas the presence of aperture provides the Furthermore, in most cases nonlinear refraction does not occur on its own, but usually in conjunction with nonlinear absorption. Using the division method, by taking the ratio of closed aperture Z-scan data to the open aperture Z-scan data, we can evaluate the pure non-linear refraction. In the present case, the curves exhibit a pre-focal transmittance maximum (peak) followed by a post-focal transmittance minimum (valley), which is similar for all the nanostructures.

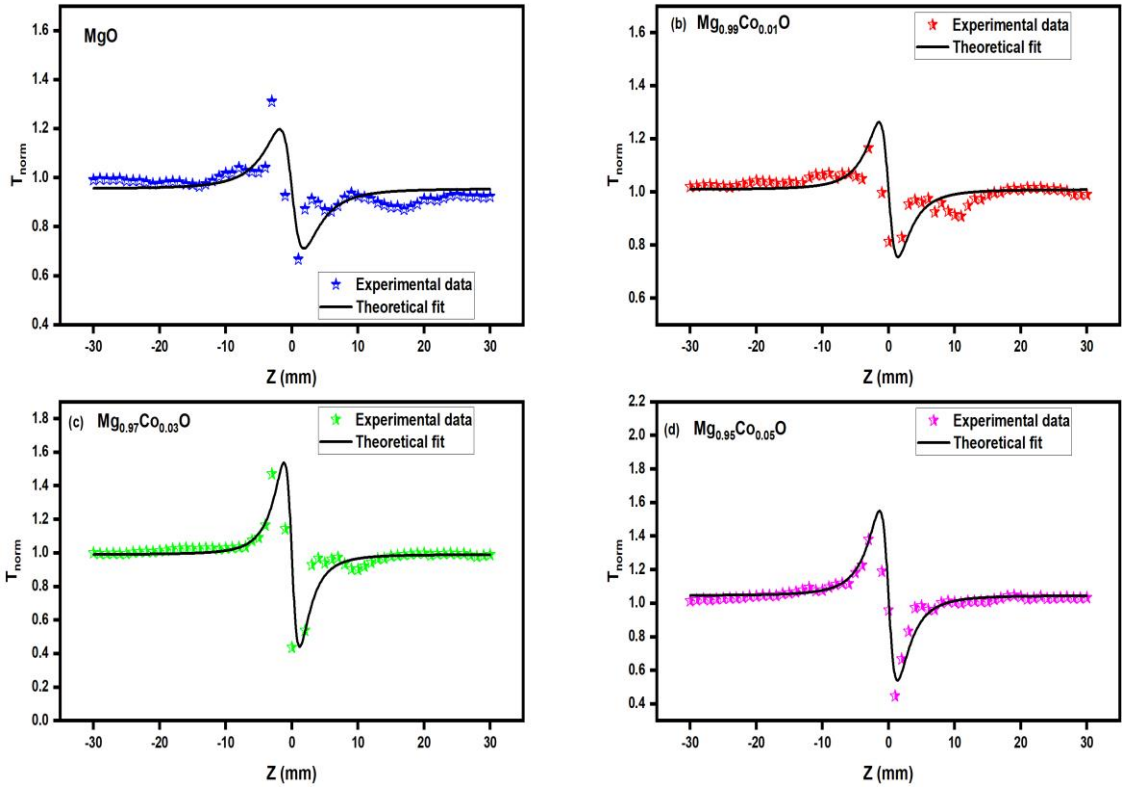

Fig. 3.8 Closed aperture Z-scan data of $Mg_{(1-x)}Co_xO$ $(x = 0, 0.01, 0.03, 0.05)$

This peak-valley criterion in closed aperture results denotes the self-defocusing property, which in turn is attributes to the negative nonlinear refractive index [6]. Moreover, the sign of the nonlinear refractive index of a sample also attains significance and it can be easily determined from the shape of the graph. There are different reasons for the origin of nonlinear

refraction like electronic, molecular, electrostrictive, or thermal mechanisms. As the present investigation is done in a continuous wave regime, the nonlinearity is thermal in origin [7]. If the peak-valley separation in the closed aperture Z-scan is more than 1.7 times the Rayleigh range (Z_R), it's a clear indication of thermal nonlinearity.

Table.3.3. Nonlinear parameters of $Mg_{(1-x)}Co_xO$ $(x = 0, 0.01, 0.03, 0.05)$under continuous wave laser

Sample	n_0	$n_2 * 10^{-9}$ (cm^2/W)	$\beta * 10^{-4}$ (cm/W)
MgO	**1.1907**	**4.03**	**1.12**
$Mg_{0.99}Co_{0.01}O$	**1.1909**	**4.37**	**2.41**
$Mg_{0.97}Co_{0.03}O$	**1.2207**	**5.03**	**2.70**
$Mg_{0.95}Co_{0.05}O$	**1.2744**	**5.75**	**3.06**

According to the observed results, both nonlinear parameters are linearly dependent on the dopant concentrations within the range studied. It has been found that the absorptive and refractive nonlinearities are enhanced with the increase in concentration of dopant. This increment may be related to the addition of dopant involved in the interaction between light and matter. As the present work deals with the cw regime, a small portion of the incident laser energy gets absorbed by the particles. On further increase in the concentration, more dopants are thermally agitated because of the local heating of the absorbed medium, which in turn results in the temperature variation of the sample medium.

Chapter-4

Conclusion and Future scope

4.1 Conclusion

Nonlinear optical semiconductor materials are of great importance, as they alter the optical properties of light propagating through them and hence they are used in many applications such as all optical signal processing, optoelectronic devices, optical switching, optical image processing, optical information storage, optical limiting, optical waveguides, high speed optical communication networks, and future applications in biological and medical sciences. Researchers are now focusing on the development of low-cost, non-toxic, and sustainable materials for the development of nonlinear optics. Over the past few decades, many materials have been considered as effective materials in applications of nonlinear optics. In the last decades, transition metal (TM) oxide nanomaterials received significant attention because of their great chemical and physical characteristics. Among this, MgO has emerged as one of the promising materials due to its unique properties such as high mechanical and chemical stability, excellent electrical and optical properties together with its natural abundance and non-toxicity. MgO have potential application in electronics, spintronics, optoelectronics, optical bistability, solar cells, gas sensors and information technology devices including displays and wavelength selective applications. A key requirement for advancing the technological uses of MgO is improved control of doping . However, a little is known about the nonlinear optical properties of MgO nanoparticles and co doped MgO nanoparticles. This necessitates the need for protecting the optical sensors and human eyes from high intense laser beams. In this article, we report for first time the third-order optical nonlinearity and optical power limiting properties of Co doped MgO nanoparticles under cw laser using Z-scan technique.

MgO and Co- doped MgO with cubic structure were synthesized via the modified auto-combustion method. Structural, morphological, and optical aspects together with third order optical nonlinearity were investigated. The crystallite size of $Mg_{(1-x)}Co_xO$ $(x = 0, 0.01, 0.03, 0.05)$were calculated as 10.62 nm, 12.48 nm, 13.19 nm, 13.52 nm respectively. XRD pattern were well matched with the standard date [JCPDS - card no 74-1225] without any other impurity phase other than dopants concentrations and having the space group *fm-3 m*. Rietveld refinement confirms the structural parameters of the prepared nanoparticles. FE-SEM images confirmed nanostructures with slightly agglomerated nature having flower petal

like morphology. Chemical composition of the nanostructures is evaluated by using energy dispersive spectrum, confirms the presence of elements like magnesium, oxygen for pristine MgO and magnesium, cobalt, oxygen for doped samples. Absence of foreign elements or impurities shows the phase purity of the nano-sized structures. Linear optical behaviour of $Mg_{(1-x)}Co_xO$ $(x = 0, 0.01, 0.03, 0.05)$ can be identified from the UV-Visible absorbance spectrum. Using the Tauc plot calculations, bandgaps are evaluated and found to be decreasing with doping concentrations. Presence of defects in the nanomaterial creates some intermediate level which in turn leads to the decrease in bandgap on doping. The third order nonlinear properties of the prepared nanoparticles were measured using the Z-scan method under diode plumbed continuous wave laser with 532 nm wavelength. Open aperture and closed aperture Z-scan measurements reveal that all samples exhibit high nonlinear absorption and nonlinear refraction. In open aperture Z-scan technique, combined effect of saturable absorption and reverse saturable absorption is observed on doping. On the other hand a self-defocussing nature with negative refractive index is observed under closed aperture Z-scan method. This study brings out Pristine MgO and Co-doped MgO as superior candidates for the fabrication of optical limiting devices for protecting human eyes and other sensitive optical detectors from hazardous laser radiation.

4.2 Future Scope

The current research investigation can be extended in the following directions:

- In order to understand more about the morphology of the prepared nanoparticles, transmission electron microscopic (TEM) techniques can be used.
- By changing the doping concentration of cobalt we can understand the structural and optical properties of MgO on doping.
- Dopant can be varied.
- By using pulsed laser with 5 ns was used as the source of excitation and there by studies can be extended to more excitation regimes, using 100 femto-second etc. laser pulses.
- The present linear and nonlinear optical studies here were analysed with the sample in liquid form. The studies can be performed with the sample in thin film form, to understand the improvement in its properties.

[1]

References

[1] S. Abed, H. Djaaboube, K. Waszkowska, K. E. Korchi, R. Aouati and A. Bouabellou, "Third Order Nonlinear Optical Properties of MgO Doped Co Thin Films by Dip Coating Technique," 2019 21st International Conference on Transparent Optical Networks (ICTON), 2019, pp. 1-4, doi: 10.1109/ICTON.2019.8840172.

[2] Abrinaei, F. (2017). Nonlinear optical response of Mg/MgO structures prepared by laser ablation method. Journal of the European Optical Society-Rapid Publications, 13(1), 1-10.

[3] Pourmostafa, D., Tajalli, H., Vahedi, A., & Milanchian, K. (2022). MgO nanoparticle effect on nonlinear refractive index of nematic liquid crystal doped with Sudan black B dye using of Z-scan method.

[4] Rad, A. S., & Ayub, K. (2018). Nonlinear optical, IR and orbital properties of Ni doped MgO nanoclusters: A DFT investigation. Computational and Theoretical Chemistry, 1138, 39-47.

[5] Tamgadge, Y. S., Muley, G. G., Thakre, N. B., Khangar, S. V., Ganorkar, R. P., & Bakale, R. Y. (2021, December). Synthesis and Nonlinear Optical Absorption of L-Valine Capped Zn-Doped MgO Nanoparticles. In Macromolecular Symposia (Vol. 400, No. 1, p. 2100021).

[6] Nadafan, M., Malekfar, R., Dehghani, Z., & Allahabadi, M. (2015). Assessment of nonlinear optical properties of polyurethane/MgO nanocomposites. Engineering and Technology Journal, 33(7 Part (B) Scientific).

[7] Raju, C. S. K., Mamatha, S. U., Rajadurai, P., & Khan, I. (2019). Nonlinear mixed thermal convective flow over a rotating disk in suspension of magnesium oxide nanoparticles with water and EG. The European Physical Journal Plus, 134(5), 196.

[8] Sahmani, S., Saber-Samandari, S., Khandan, A., & Aghdam, M. M. (2019). Influence of MgO nanoparticles on the mechanical properties of coated hydroxyapatite nanocomposite scaffolds produced via space holder technique: fabrication,

characterization and simulation. Journal of the mechanical behavior of biomedical materials, 95, 76-88.

[9] Sahmani, S., Saber-Samandari, S., Khandan, A., & Aghdam, M. M. (2019). Influence of MgO nanoparticles on the mechanical properties of coated hydroxyapatite nanocomposite scaffolds produced via space holder technique: fabrication, characterization and simulation. Journal of the mechanical behavior of biomedical materials, 95, 76-88.

[10] Nadafan, M., Dehghani, Z., Faraji Alamouti, A., & Vejdani Noghreiyan, A. (2022). The influence of gamma irradiation on linear and nonlinear optical properties of magnesium oxide nanoparticles via Z-scan technique. Journal of the Australian Ceramic Society, 58(1), 249-258.

[11] Kalhori, E. M., Al-Musawi, T. J., Ghahramani, E., Kazemian, H., & Zarrabi, M. (2017). Enhancement of the adsorption capacity of the light-weight expanded clay aggregate surface for the metronidazole antibiotic by coating with MgO nanoparticles: Studies on the kinetic, isotherm, and effects of environmental parameters. Chemosphere, 175, 8-20.

[12] Rana, P., Gupta, S., & Gupta, G. (2022). Unsteady nonlinear thermal convection flow of MWCNT-MgO/EG hybrid nanofluid in the stagnation-point region of a rotating sphere with quadratic thermal radiation: RSM for optimization. International Communications in Heat and Mass Transfer, 134, 106025.

[13] Nadafan, M., Dehghani, Z., Faraji Alamouti, A., & Vejdani Noghreiyan, A. (2022). The influence of gamma irradiation on linear and nonlinear optical properties of magnesium oxide nanoparticles via Z-scan technique. Journal of the Australian Ceramic Society, 58(1), 249-258.

[14] Igwegbe, C. A., Banach, A., & Ahmadi, S. (2018). Adsorption of reactive blue 19 from aqueous environment on magnesium oxide nanoparticles: kinetic, isotherm and thermodynamic studies. Pharm Chem J, 5, 111-121.

[15] Nadafan, M., Malekfar, R., & Dehghani, Z. (2015). Determination of nonlinear optical properties of MgO nanoparticles doped in poly (Ether) urethane. Acta Phys. Pol. A, 128, 29-33.

[16] Basavaraj, B., Pushpanjali, G. M., & Sannakki, B. (2021). STUDIES ON OPTICAL BEHAVIOR OF CONDUCTING POLYMER OLYANILINE WITH MGO NANOPARTICLES. STUDIES.

[17] SAFAEI, G. J., Zahedi, S., Javid, M., & Ghasemzadeh, M. A. (2015). MgO nanoparticles: an efficient, green and reusable catalyst for the onepot syntheses of 2, 6-dicyanoanilines and 1, 3-diarylpropyl malononitriles under different conditions.

[18] Chandran, A., Prakash, J., Naik, K. K., Srivastava, A. K., Dąbrowski, R., Czerwiński, M., & Biradar, A. M. (2014). Preparation and characterization of MgO nanoparticles/ferroelectric liquid crystal composites for faster display devices with improved contrast. Journal of Materials Chemistry C, 2(10), 1844-1853.

[19] Abrinaei, F. (2017). Nonlinear optical response of Mg/MgO structures prepared by laser ablation method. Journal of the European Optical Society-Rapid Publications, 13(1), 1-10.

[20] M. Sheik-bahae, A. L. I. A. Said, and T. Wei, "Sensitive Measurement of Optical Nonlinearities Using a Single Beam," vol. 26, no. 4, 1990.

[21] G. S. Boltaev, R. A. Ganeev, P. S. Krishnendu, K. Zhang, and C. Guo, "Nonlinear optical characterization of copper oxide nanoellipsoids," *Scientific Reports*, pp. 1–8, 2019, doi: 10.1038/s41598-019-47941-8.

[22] H. Search, C. Journals, A. Contact, M. Iopscience, L. Phys, and I. P. Address, "Structural , photoinduced optical effects and third-order nonlinear optical studies on Mn doped and Mn – Al codoped ZnO thin films under continuous wave laser irradiation," vol. 035404, doi: 10.1088/1054-660X/24/3/035404.

[23] [A. A. Aboud, A. Salah, and A. Saad, "Effect of heavy metals (Ni , Cu , Pb) doped ZnO on the nonlinear optical properties Effect of heavy metals (Ni , Cu , Pb) doped

ZnO on the nonlinear optical properties Manuscript version : Accepted Manuscript," no. November, 2020, doi: 10.1088/2053-1591/abc845.

[24] S. Dhanuskodi, T. C. Sabari Girisun, and S. Vinitha, "Optical limiting behavior of certain thiourea metal complexes under CW laser excitation," *Current Applied Physics*, vol. 11, no. 3, pp. 860–864, 2011, doi: 10.1016/j.cap.2010.12.009.

[25] L. K. Joy, M. George, J. Alex, A. Aravind, D. Sajan, and G. Vinitha, "Twisted intramolecular charge transfer investigation of semi organic L-Glutamic acid hydrochloride single crystal for organic light-emitting and optical limiting applications," *Journal of Molecular Structure*, vol. 1156, pp. 733–744, 2018, doi: 10.1016/j.molstruc.2017.11.126.

[26] S. Elizabeth *et al.*, "Nonlinear optical and photocatalytic dye degradation of Co doped CeO 2 nanostructures synthesized through a modi fi ed combustion technique," *Ceramics International*, vol. 46, no. 9, pp. 13932–13940, 2020, doi: 10.1016/j.ceramint.2020.02.189.

[27] Afrand, M., Abedini, E., & Teimouri, H. (2017). How the dispersion of magnesium oxide nanoparticles effects on the viscosity of water-ethylene glycol mixture: experimental evaluation and correlation development. Physica E: Low-dimensional Systems and Nanostructures, 87, 273-280.

[28] M. Sheik-bahae, A. L. I. A. Said, and T. Wei, "Sensitive Measurement of Optical Nonlinearities Using a Single Beam," vol. 26, no. 4, 1990.

[29] G. S. Boltaev, R. A. Ganeev, P. S. Krishnendu, K. Zhang, and C. Guo, "Nonlinear optical characterization of copper oxide nanoellipsoids," *Scientific Reports*, pp. 1–8, 2019, doi: 10.1038/s41598-019-47941-8.

[30] H. Search, C. Journals, A. Contact, M. Iopscience, L. Phys, and I. P. Address, "Structural , photoinduced optical effects and third-order nonlinear optical studies on Mn doped and Mn – Al codoped ZnO thin films under continuous wave laser irradiation," vol. 035404, doi: 10.1088/1054-660X/24/3/035404.

[31] A. A. Aboud, A. Salah, and A. Saad, "Effect of heavy metals (Ni , Cu , Pb) doped ZnO on the nonlinear optical properties Effect of heavy metals (Ni , Cu , Pb) doped ZnO on

the nonlinear optical properties Manuscript version : Accepted Manuscript," no. November, 2020, doi: 10.1088/2053-1591/abc845.

[32] S. Dhanuskodi, T. C. Sabari Girisun, and S. Vinitha, "Optical limiting behavior of certain thiourea metal complexes under CW laser excitation," *Current Applied Physics*, vol. 11, no. 3, pp. 860–864, 2011, doi: 10.1016/j.cap.2010.12.009.

[33] L. K. Joy, M. George, J. Alex, A. Aravind, D. Sajan, and G. Vinitha, "Twisted intramolecular charge transfer investigation of semi organic L-Glutamic acid hydrochloride single crystal for organic light-emitting and optical limiting applications," *Journal of Molecular Structure*, vol. 1156, pp. 733–744, 2018, doi: 10.1016/j.molstruc.2017.11.126.

[34] S. Elizabeth *et al.*, "Nonlinear optical and photocatalytic dye degradation of Co doped CeO 2 nanostructures synthesized through a modi fi ed combustion technique," *Ceramics International*, vol. 46, no. 9, pp. 13932–13940, 2020, doi: 10.1016/j.ceramint.2020.02.189.